의학박사 학위논문

심근세포의 신경형 산화질소 합성효소 접합변이체 발현 양상과 고혈압에서 심근보호의 새로운 기전 연구

Neuronal nitric oxide synthase splicing variants and their novel mechanisms of myocardial protection in hypertensive heart

2017 년 02 월

서울대학교 대학원
의과학과 의과학전공
장 지 현

A thesis of the Degree of Doctor of Philosophy

Neuronal nitric oxide synthase splicing variants and their novel mechanisms of myocardial protection in hypertensive heart

심근세포의 신경형 산화질소 합성효소 접합변이체 발현 양상과 고혈압에서 심근보호의 새로운 기전 연구

February 2017

The Department of Biomedical Sciences,
Seoul National University
College of Medicine
Ji Hyun Jang

심근세포의 신경형 산화질소 합성효소 접합변이체 발현 양상과 고혈압에서 심근보호의 새로운 기전 연구

지도 교수 장 은 화

이 논문을 의학박사 학위논문으로 제출함

2016 년 10 월

서울대학교 대학원
의과학과 의과학전공
장 지 현

장지현의 의학박사 학위논문을 인준함

2016 년 12 월

위 원 장 _____ (인)
부위원장 _____ (인)
위 원 _____ (인)
위 원 _____ (인)
위 원 _____ (인)

Neuronal nitric oxide synthase splicing variants and their novel mechanisms of myocardial protection in hypertensive heart

by
Ji Hyun Jang

A thesis submitted to the Department of Biomedical Sciences in partial fulfillment of the requirements for the Degree of Doctor of Philosophy in Medical Science at Seoul National University College of Medicine

December 2016

Approved by Thesis Committee:

Professor _____Chairman

Professor _____Vice chairman

Professor _____

Professor _____

Professor _____

ABSTRACT

Cardiac nNOS is well established to be an intracellular Ca^{2+} modulator and regulates myocardial contractility in healthy and diseased hearts. Importantly, previous work from our research group has shown that nNOS is up-regulated in the cytosol/membrane of the myocardium in hypertension and promotes lusitropy through myofilament Ca^{2+} desensitiztion of cardiac myocytes. Until recently, the mechanisms mediating nNOS up-regulation by pathological stimuli and the mechanisms of cardiac protection in hypertension by nNOS are not fully understood. My recent work has shown that angiotensin II (Ang II, 1 μM, 3 hrs) increased nNOS protein expression and activity in rat cardiac myocytes subsequent to AT1R/NADPH oxidase activation. Intriguingly, Ang II increased endothelial NOS (eNOS) Ser^{1177} and decreased eNOS Thr^{495} *via* NADPH oxidase-derived reactive oxygen species (ROS); NOS inhibition (LNG-Nitroarginine Methyl Ester, L-NAME) or eNOS gene deletion ($eNOS^{-/-}$) abolished AT2R translocation to plasma membrane and Ang II-induced nNOS protein expression. AT2R was S-nitrosated by NO, site-specific mutagenesis analysis and

immunocytochemistry using confocal microscopy revealed the importance of C-terminal Cys^{349} residue in AT2R translocation to plasma membrane, suggesting that eNOS may have increased the *S*-nitrosation and activation of AT2R through Cys^{349}.

Next, I aimed to investigate the molecular mechanisms mediating nNOS protection in the myocardium of hypertensive rats. Immunohistochemistry experiments confirmed that chronic inhibition of nNOS with the specific inhibitor, S-methyl-L-thiocitrulline (SMTC) *in vivo* induced cardiac hypertrophy and intermittent fibrosis in Ang II-induced hypertensive rat (SMTC+Ang II) with little effect in Sham. In echocardiography, LV septum, posterior wall thickness and the ejection fraction were increased but the end-diastolic and systolic chamber dimension were reduced in SMTC+Ang II compared to Sham, SMTC and Ang II. Transmission electron microscopy showed that the lengths of sarcomere and I-band but not the length of thick filament of the myocardium were significantly elongated in SMTC+Ang II. Fluorescent microscopic imaging confirmed the elongation of the sarcomere and Z-disc of LV myocytes from SMTC+Ang II. Immunoblotting experiments showed that the abundance of nebulette was increased but troponin I was reduced

and the rest of the thick, thin and Z-disc proteins were not different after nNOS inhibition. Functionally, slack sarcomere lengths were increased before myocyte contraction in SMTC+Ang II. However, at steady-state contraction with field stimulation (2 Hz), the difference in sarcomere length was absent and the diastolic and systolic Ca^{2+} transient amplitudes were increased with nNOS inhibition. Myofilament Ca^{2+} sensitivity, which is reduced in hypertension by nNOS, was significantly increased in SMTC+Ang II. Furthermore, immunoblotting from the myofilament fraction of cardiac myocytes demonstrated the expression of nNOSβ (M.W. ~140 kDa) in LV myocytes from Sham and hypertensive rats (which was distinct from nNOSα/μ, M.W. 155~165 kDa, in the plasma membrane/cytosol). Albeit with reduced intensity, nNOSβ protein expression was detected in the myofilament of cardiac myocytes from nNOSα/μ null mice. The protein expression of nNOSβ was significantly increased in SMTC and SMTC+Ang II in rats. Myofilament proteins were not affected by nNOSα/μ gene deletion.

Taken together, I have revealed, *for the first time*, the cross talk between AT1R and AT2R on nNOS up-regulation *via* NADPH oxidase/ROS-stimulation of eNOS activity in cardiac

myocytes. Using a hypertensive model with nNOS inhibition, I have demonstrated that nNOS is essential in maintaining sarcomere structure and function of cardiac myocyte, protects the heart from cardiac hypertrophy and fibrosis in hypertension. Importantly, I have identified a novel splice variant of nNOS, nNOSβ, in the myofilament fraction of cardiac myocyte. nNOSα/μ and nNOSβ−regulation of myofilament structure and kinetics will shed light on a new conceptual framework for better understanding of the hypertrophic progression and nNOS protection of the heart under stress.

Some of the works are published in *Basic Res Cardiol* (2015) 110(3):21., and *Nitric Oxide* (2015) 11;50:20−27.

Keywords: nNOS splice variant, cardiac protection, hypertension, sarcomere, myofilament, heart
Student number: 2013−30617

CONTENTS

LIST OF TABLES AND FIGURES

Chapter 1

Chapter 2

PART 1.

LIST OF ABBREVIATIONS

NO: Nitric Oxide

nNOS: Neuronal nitric oxide synthase

eNOS: Endothelial nitric oxide synthase

L−NAME: n(omega)−nitro−L−arginine methyl ester

SMTC: S−methyl−L−thiocitrulline

Ang II: Angiotensin II

AT2R: Angiotensin II type 2 receptor

AT1R: Angiotensin II type 1 receptor

SNP: Sodium Nitroprusside

LV: Left Ventricle

HP: Hypertension

WGA: Wheat Germ Agglutinin

DAPI: 4', 6'−Diamidino−2−phenylindole

nNOSα/μ: nNOS alpha or nNOS mu splicing variant

Tn I: Troponin I

cMyBPC: cardiac myosin binding protein C

PKG: Protein kinase G

cGMP: Cyclic guanosine monophosphate

PP2A: Protein phosphatase 2A

GENERAL INTRODUCTION

1. Nitric oxide and nitric oxide synthases in cardiovascular system

Nitric oxide (NO) is an ubiquitous signaling molecule that is expressed in almost all tissues and cells in the biological system which is involved in the growth, proliferation, metabolism and muscle contractility, etc. (Alderton, Cooper et al. 2001). In the cardiovascular system, bioavailability of NO has been implicated in the regulation of various functions including vascular smooth muscle relaxation and platelet inhibition (Ignarro, Harbison et al. 1986). In the heart, it is well known that NO, which is generated in the heart tissue, activates a number of signaling pathways, regulates intracellular calcium handling and affects myocardial contractility (Bohlen 2015). In particular, NO promotes diastolic relaxation of left ventricle (LV) and serves to lower the pressure in the LV chamber (Paulus, Vantrimpont et al. 1994, Matter, Mandinov et al. 1999, Paulus 2000).

Basically, there are three NO synthases (NOSs), two are constitutive NOSs (neuronal NOS, nNOS; endothelial NOS, eNOS) and the other is inducible NOS (iNOS, induced by cytokines

during inflammation). Constitutive NOS, nNOS & eNOS, share the same mechanism for the activation in the cardiac muscle of mammals, e.g. NOSs are Ca^{2+}/calmodulin-activated enzymes (Alderton, Cooper et al. 2001). However, compelling evidences show that nNOS and eNOS are located diversely in the same myocyte (Mungrue and Bredt 2004) and exert different functions in Ca^{2+} homeostasis and cardiac contractility (Xu, Huso et al. 1999, Barouch, Harrison et al. 2002, Sears, Bryant et al. 2003, Zhang and Casadei 2012, Zhang, Jin et al. 2014). For example, eNOS is located in the caveolae under normal condition (Feron, Belhassen et al. 1996) and eNOS is shown to translocate to the cytosol and regulates ryanodine receptors (RyR) with stimulation (Petroff, Kim et al. 2001). On the other hand, nNOS is located in the SR (Xu, Huso et al. 1999, Bendall, Damy et al. 2004) and in the plasma membrane (Ueda, Valdivia et al. 2008) and regulates Na^{+} and Ca^{2+} homeostasis in cardiac myocytes. Importantly, whilst eNOS is "uncoupled" and becomes the source of ROS in the myocardium under pressure-overload (Takimoto, Champion et al. 2005) or it is downregulated in the failing heart (Wiemer, Itter et al. 2001), nNOS is upregulated and prevents the myocardium from oxidative stress, adverse remodeling and

delays the pathological progression towards heart failure (Bendall, Damy et al. 2004, Damy, Ratajczak et al. 2004, Jin, Jang et al. 2013).

2. Downstream molecular mechanisms of nNOS in healthy and diseased hearts

It has been demonstrated during the past decades that nNOS regulates the excitation-contraction coupling, intracellular calcium handling, redox homeostasis and post-transcriptional modification involving various phosphatase/kinases in cardiomyocytes (Zhang, Jin et al. 2014). As shown in Fig. 1, nNOS modulates the activities of L-type Ca^{2+} channel (Sears, Bryant et al. 2003) and voltage-gated Na^{+} channel (Ueda, Valdivia et al. 2008) (restrict Na^{+} and Ca^{2+} influx into the cardiomyocytes); reduces intracellular Ca^{2+} transients and attenuates myocardial contractility and arrhythmogenesis in diseased heart (Gonzalez, Beigi et al. 2007). On the other hand, nNOS promotes Ca^{2+} reuptake into SR via Ca^{2+}-ATPase (SERCA) subsequent to phospholamban phosphorylation, through protein phosphatase (PP1 or PP2A)-dependent and PKA-mediated phosphorylation resulting in the facilitation of

myocardial relaxation (Zhang, Zhang et al. 2008). Alternatively, NO may directly or indirectly affect the S-nitrosation or oxidation of thiol groups in cysteine residues of nNOS targeting proteins, such as SERCA, L-type Ca^{2+} channel and RyR 2 (Adachi, Weisbrod et al. 2004, Burger, Lu et al. 2009). Moreover, in both healthy and diseased hearts, nNOS has been shown to attenuate the activities of NADPH oxidase in sarcolemma membrane (Zhang, Dingle et al. 2009, Jin, Jang et al. 2012), xanthine oxidoreductase (Kinugawa, Huang et al. 2005) or mitochondrial oxidases (Burkard, Williams et al. 2010) to modulate oxidative stress. Recent research from our group has showed that nNOS-derived NO affects downstream target proteins through soluble guanylate cyclase (sGC)-dependent and cGMP/protein kinase G (PKG)-mediated phosphorylation of myofilament proteins (Jin, Jang et al. 2012). In addition, nNOS influences myofilament Ca^{2+} sensitivity in cardiomyocytes from healthy and hypertensive rat hearts (Jin, Jang et al. 2013). However, whether nNOS is functionally expressed in the myofilament of cardiomyocytes is unknown. In the studies from our group and that of others, nNOS protein expression and activity are shown to be increased in hypertension, hypertrophic

and failing myocardium where nNOS-derived NO is responsible for the "maintenance" of myocardial NO and suppresses the sources of cardiac oxidative stress. Accumulating evidence indicates that increased protein expression and activity of nNOS in ischaemia/reperfusion injury, infarct, hypertrophic or failing myocardium are important protective mechanisms in reversing oxidative stress and contractile dysfunction (Takimoto, Aoyama et al. 2002, Damy, Ratajczak et al. 2003, Bendall, Damy et al. 2004, Damy, Ratajczak et al. 2004, Dawson, Lygate et al. 2005, Sun, Picht et al. 2006, Burger, Lu et al. 2009, Aragon, Condit et al. 2011, Niu, Watts et al. 2012). Until recently, the mechanism mediating nNOS up-regulation in the heart under stress remains unidentified. In *Chapter 1*, I have identified a novel mechanism leading to nNOS upregulation by Ang II.

3. Splicing variants of nNOS

A number of nNOSs are known to be produced from alternate splicing nNOS mRNA variants, namely nNOSα, nNOSβ, nNOSγ, nNOSμ and nNOS2 (Fig. 2) (Eliasson, Blackshaw et al. 1997). Recent consensus is that various splice variants of nNOS are expressed in discrete organelles in the same cell types (Percival,

Anderson et al. 2010). nNOSα, which contains a PDZ domain (postsynaptic density-95 (PSD-95)/Discs large/zona occludens-1) in N-terminus and targets to the plasma membrane, is concentrated at the synaptic junction in the brain and regulates the dynamics of neuronal synapses (Mungrue and Bredt 2004). nNOSμ, which contains 34 additional amino acids, has been shown to be expressed in the brain, prevalently in mesencephalon and the cerebellum (Ihara, Kuwamura et al. 2006). Subsequently, nNOSβ, nNOSγ and nNOS2 are shown to be present in the same areas of the brain (Eliasson, Blackshaw et al. 1997, Iwasaki, Hori et al. 1999, Putzke, Seidel et al. 2000). Similarly, both nNOSμ and nNOSβ are expressed in skeletal muscle cells or nNOSα and nNOSβ are in collecting duct or cortex of kidney (Smith, Merchant et al. 2009, Lu, Fu et al. 2010, Percival, Anderson et al. 2010). nNOSμ is located in sarcolemma membrane in the myocardium or in skeletal muscle, exerts a key part in muscle contractility, especially during exercise (Mungrue and Bredt 2004). Conversely, nNOSβ lacks the PDZ domain and localizes in the cytosol (Golgi) in skeletal muscle (Percival, Anderson et al. 2010). Importantly, splice variants of nNOS in discrete locations exert different functions: e.g. nNOSμ is

involved in muscular blood supply or angiogenesis during mechanical demand whereas nNOSβ is involved in the structural integrity for the optimal force generation (Percival, Anderson et al. 2010). Furthermore, N-terminal of nNOSα and μ interacts with other proteins (e.g α-syntrophin) *via* PDZ binding motif, involving functional regulation of its interacting protein through the maintenance of NO in specific location of cardiac myocyte. Likewise, spatial compartmentalization of nNOS is critical to the local NO to exert function, due to the high concentration of the powerful NO scavenger such as myoglobin and glutathione in cardiac muscle (Flogel, Merx et al. 2001). However, whether nNOSβ splice variant is also expressed in cardiomyocytes and if so, the location of its expression has not been reported yet. In many other tissues, nNOSβ, which remains NOS activity to produce NO, is shown to exert diverse effects, such as 1) protect the renal cortex from oxidative stress (Cunningham, Sasser et al. 2013) 2) mediates signaling for penile erection (Hurt, Sezen et al. 2006) 3) increases the resistance of skeletal muscle fatigue (Bernardo, Weeks et al. 2010). In skeletal muscle, nNOSβ in the cis-Golgi membrane is shown to activate PKG-dependent signaling mechanism that has a direct effect on the muscle force

generation through continuous NO production (Percival, Anderson et al. 2010). In addition, it was confirmed that nNOSβ contributes to the structural integrity in the skeletal muscle (Percival, Anderson et al. 2010). However, the presence or absence of nNOSβ in the myocardium as well as the molecular function of nNOSβ in healthy and diseased hearts, were unidentified.

4. NO modulation of concentric cardiac hypertrophy

Concentric and eccentric hypertrophy are the two structural remodeling of myocardium under pressure-overload (Grossman, Jones et al. 1975). In contrast to eccentric hypertrophy, where cardiac mass and the volume of the cardiac chamber are both increased, concentric hypertrophy is characterized by increased relative wall thickness, cardiac mass, but reduced volume of the cardiac chamber. Increased afterload, such as high blood pressure in hypertension or aortic stenosis and increased cytosolic Ca^{2+}, are the primary causes lead to the progression of concentric hypertrophy (Bernardo, Weeks et al. 2010, Katholi and Couri 2011). Previous research with eNOS/nNOS or eNOS null mice demonstrated the development of concentric

hypertrophy in LV, accompanied by the changes in the Ca^{2+} handling protein and cytokine (Yang, Liu et al. 1999, Barouch, Cappola et al. 2003, Flaherty, Brown et al. 2007). Nevertheless, myocardial structure was remained unchanged in nNOSα/μ null mice. Myocardial infarction in nNOSα/μ null mice, however, induced cardiac structural modelling, systolic and diastolic functional deterioration with reduced beta-adrenergic reserve (Dawson, Lygate et al. 2005). Taken together, up-regulation of nNOS to maintain the bioavailability of NO in diseased heart and understanding the underlying mechanisms of nNOS in the regulation of cardiac structure, especially in hypertension is important to prevent the pathological remodeling of myocardium under pressure overload. In *chapter 2*, I investigated whether the chronic inhibition of nNOS affects the structure and function of the myofilament of cardiac myocyte in normal heart and in hypertension.

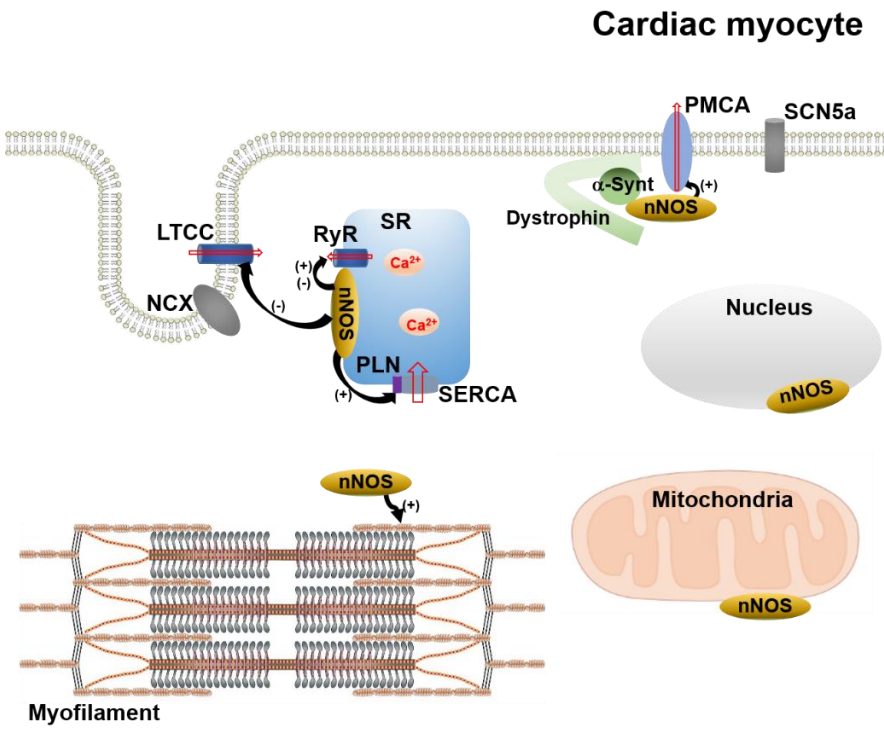

Figure 1. Schematic diagram of the localization and function of nNOS in cardiac myocyte

nNOS, which is expressed in intracellular organelles in cardiac myocyte, such as SR, mitochondria, nucleus and plasma membrane, regulates intracellular Ca^{2+} handling (red arrow) and functions of the particular organelles *via* generating NO in the respective compartments. Black arrow indicates activation (+) or inhibition (−) of target proteins. α−Synt: α−Syntrophin, PMCA: Plasma membrane Ca^{2+} ATPase, SCN5A: Sodium voltage−gated channel alpha subunit 5, SR: Sarco/Endoplasmic reticulum, SERCA: Sarco/endoplasmic reticulum Ca^{2+}−ATPase, RyR: Ryanodine receptor, LTCC: L−type Ca^{2+} channel, NCX: Na^{+}−Ca^{2+} exchanger, PLN: Phospholamban.

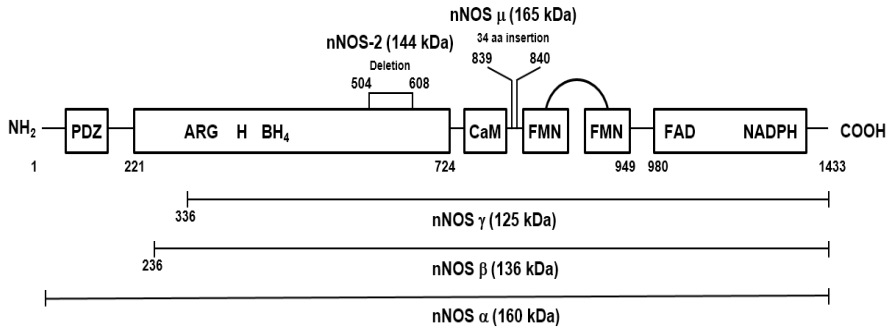

Figure 2. Structure of the splicing variants of nNOS

nNOS is composed of one oxygenase and one reductase domain with Ca^{2+}−calmodulin binding site. There are five alternative splicing variants of nNOS, which are distinctive in molecular weight (nNOS α, μ, β, γ, −2).

MATERIALS AND METHODS

1. Animals

Sprague-Dawley rats (12 weeks old, male) were used in the current project. Sprague-Dawley rats (8 weeks old, male) were randomly divided into four groups designated to be the Sham, SMTC, Ang II and SMTC+Ang II-infused rats. Briefly, rats were anesthetized with isoflurane (2.5 %), and an osmotic minipump (Alzet model 2004) containing SMTC (infusion rate: 28 ng/min/kg) and Ang II (infusion rate: 125 ng/min/kg) were implanted in the midscapular region under sterile condition. Sham-operated animals underwent the same surgical procedure, except for no pump insertion.

Blood pressure was measured every other day from day -3 using Non-Invasive Blood Pressure System, tail-cuff method (CODA). Rats were warmed at 37 ℃ for 15 minutes before the measurement; blood pressure and heart rate parameters are the means of ten readings.

In some experiments, $eNOS^{+/+}$ and $eNOS^{-/-}$ mice (*Tohoku University Graduate School of Medicine*) and nNOSα/μ null mice (male, 3-4 months old, Jackson Laboratory, Strain number:

B6.129S4-*Nos1*^{tm1Plh}/J, obtained from Dr. Su-Cheong Yeom, *Seoul National University*) were used for experiments.

The study protocol was in accordance with the Guide for the Care and Use of Laboratory Animals by the US National Institutes of Health (NIH Publication No. 85-23, revised 1996), and also conforms to the Institutional Animal Care and Use Committee (IACUC) in Seoul National University (IACUC approval No.: SNU-101012-3).

2. Isolation of left ventricular myocytes

Rats (normal, Sham, Ang II, SMTC and SMTC+Ang II) were anesthetized with pentobarbital sodium (30 mg/kg, i.p.) and the mice were humanely killed with cervical dislocation. Briefly, the hearts from rats and mice were extracted and mounted onto the Langendorff perfusion system and was perfused with a nominal Ca^{2+}-free solution (in mM; NaCl 135, KCl 5.4, $MgCl_2$ 3.5, glucose 5, HEPES 5, Na_2HPO_4 0.4, Taurine 20 at a pH of 7.4), followed by a further 8 min with enzymes added (collagenase, 1 mg/ml, Worthington Biochemical Co.; protease, 0.133 mg/ml, Sigma Aldrich; BSA 1.65 mg/ml; Ca^{2+}, 0.05 mM, Sigma). Myocytes were harvested from LV chamber of the heart following further

five and ten minutes digestion periods in a separate flask containing fresh collagenase-only solution, washed and re-suspended in storage solution (in mM; NaCl 120, KCl 5.4, $MgSO_4$ 5, $CaCl_2$ 0.2, Na^+-pyruvate 5, glucose 5.5, Taurine 20, HEPES 10, Mannitol 29, pH 7.4, NaOH). The myocyte suspension was stored at RT and cells were used within 8 hrs of isolation.

3. Isolation of the membrane/cytosol and the myofilament fractions of LV myocytes

Membrane/cytosol fraction was extracted from LV myocytes using lysis buffer contained 0.5 M EDTA, 25 mM Tris-HCl, 150 mM NaCl, 1% Triton X-100 with phosphatase & protease inhibitor cocktail (Roche), pH 7.4. To obtain myofilament fraction, LV myocytes were washed with cold phosphate-buffered saline (PBS) and were transferred to screw cap tubes containing 2.3 mm zirconia/silica beads (BioSpec Products) and cold buffer (60 mM KCl, 30 mM imidazole, 2 mM $MgCl_2$ and 1 % Triton X-100 with protease and phosphatase inhibitor cocktail). Cells in lysis buffer were homogenized with a bead beater (Mini-Beadbeater-8, BioSpec Products) for 20 s and the homogenates were centrifuged at 8000 rpm for 10 min at 4 ℃. The supernatant was

discarded. This procedure was repeated at least six times. The remaining pellets (myofilament enriched fraction) were re-suspended in high salt buffer (Biorad #163-2104) and were stored at room temperature for subsequent experiments.

4. Immunoblotting

Proteins were extracted from LV myocytes, skeletal muscle and brain tissues, respectively, using lysis buffer with phosphatase inhibitor & protease inhibitor cocktail (Roche), pH 7.4. Protein concentration was determined by the Bradford assay. The protein samples were mixed 5X Laemmli' s sample buffer, loaded onto a SDS polyacrylamide gel, and transferred to polyvinylidene difluoride membranes in 25 mM Tris, 192 mM Glycine, 0.01 % SDS and 20 % methanol. Membranes were blocked in 1X TBS containing 1 % Tween-20 and 5 % BSA (blocking solution) for 1 hr at RT with gentle rocking. Membranes were then incubated overnight at 4 ℃ with each of primary antibodies (Table 1.) followed by relevant secondary antibodies after washing. Blots were developed using ECL Plus western blotting detection reagents (Amersham Bioscience) by film exposure. Membranes were stripped of antibodies using

stripping buffer (Pierce Chemical) for 15 min at RT. The relative densities were calculated by normalizing of each blot with GAPDH using with ImageJ analysis software program.

5. DNA constructs of AT2R

The AT2R wild type cloned into pEGFP-N1 was kindly provided by Dr. Guangyu Wu laboratory (*Medical College of Georgia*). Cysteine mutants at C70A, C71A, C319A, C349A in intracellular region of AT2R were generated by using QuikChange XL Site-Directed Mutagenesis Kit (Agilent Technologies). The DNA sequences were confirmed by direct sequencing.

6. Cell culture and transient transfection

HEK293T cells were cultured in Dulbecco's modified Eagle's medium (Gibco), supplemented with 10 % fetal bovine serum (FBS). Cells were maintained at 37 ℃ and 5 % CO_2. Cells were transiently transfected with 500 ng of AT2R-GFP wild type (WT), AT2R C70A-GFP, AT2R C71A-GFP, AT2R C319A-GFP and AT2R C349A-GFP mutants for 48 hrs using X-tremeGENE HP DNA transfection Reagent (Roche) according

to manufacturer's instructions.

7. Immunocytochemistry and confocal imaging

Isolated LV myocytes were attached to laminin (Sigma)-coated coverslips for 1 hr at 37 ℃. After treated with Ang II, L-NAME+Ang II or SNP for 30 min, cells were fixed with 4 % PFA for 30 min in RT and washed with PBS for three times. Fixed cells (not permeabilized) were incubated in blocking solution (5 % FBS in PBS) for 1 hr, followed by an incubation with extracellular membrane targeting anti-rabbit AT2R polyclonal antibody (1:100, Alomone labs) for overnight at 4 ℃. After three washes in PBS for 10 min, cells were incubated with Alexa Fluor 488-conjugated goat anti-rabbit (1:500, Invitrogen/Molecular Probes) for 1 hr. Finally, the cells mounted with fluorescent mounting medium (Vectashield). Similarly, HEK 293T cells (transfected with GFP-tagged wild type or mutant AT2R) were attached to twelve-well plates pre-coated with poly-L-lysine and were randomely assigned for control or SNP (10 μM for 30 min) groups. Cells were fixed with 4 % PFA for 30 min, followed by Alexa Fluor 555 conjugated Wheat Germ Agglutinin (WGA, 5.0 ug/mL, Invitrogen/Molecular Probes) and 4', 6'-Diamidino-

2-phenylindole (DAPI, sigma) for 1 min in RT. The immunostained LV myocytes and AT2R transfected HEK293T cells were imaged using a laser scanning confocal microscope (Olympus, FluoView 1000) with an oil immersion objective of 100X.

8. Surface biotinylation

AT1R and AT2R densities in the plasma membrane following Ang II stimulation (0-30 min) were detected in rat LV myocytes by using surface biotinylation method. 0.25 mg/mL Sulfo-NHE-SS-Biotin (Pierce) in PBS was added to the cell suspension and gently shaked for 1 h at 4 ℃. After quenching free biotin by adding 50 mM Tris-Cl (pH 7.4), LV myocytes were lysed in lysis buffer (0.5 M EDTA, 25 mM Tris-Cl pH 7.4, 150 mM NaCl, 1% Triton X-100) and centrifuged at 13,000 g for 10 min. Supernatants were incubated with solution containing NeutrAvidin Agarose Resins (Pierce) for 1 hr at RT. Beads were washed two times with 0.1 % TBS-T. Avidin binding proteins were eluted with elution buffer (62.5 mM Tris-Cl pH 6.8, 1 % SDS, 10 % glycerol, 50 mM DTT) and loaded onto an SDS 10 % polyacrylamide gel. Immunoblotting was performed by AT1R

(Santa Cruz Biotechnology), AT2R (Santa Cruz Biotechnology) primary antibody. AT2R surface densities in the plasma membrane following SNP treatment (30 min) were detected in AT2R transfected HEK293T cells under the same condition. Membrane expression of AT2R protein in plasma membrane was confirmed with GFP (Invitrogen/Molecular probes) antibody in immunoblotting.

9. S-nitrosation

S-nitrosation of AT2R was analyzed by biotin-switch method. S-nitrosated cysteine residues of AT2R were covalently labeled with maleimide-biotin according to the manufacturer's instructions (S-nitrosated protein detection assay kit; Cayman Chemical). Biotin-conjugated proteins were then isolated with Streptavidin-coupled Dynabeads (Life Technologies) overnight at 4 °C. After washing with PBS-T (buffer composition - 50 mM Tris-Cl, pH 8.0; 150 mM NaCl, 1 mM EDTA and 1 % Tween 20), the proteins bound to the beads were eluted by boiling for 10 min in sodium dodecyl sulfate containing buffer and the S-nitrosated proteins were subjected to SDS-PAGE and western blot analysis with AT2R antibody. S-nitrosation of AT2R was compared in LV

myocytes before and after SNP treatment.

10. Reverse transcriptase polymerase chain reaction RT-PCR

Total RNA was extracted using a TRizol reagent (Invitrogen) and its purified concentration was determined nano drop. Complementary DNA was produced using SuperScript™ III First-Strand Synthesis System (Invitrogen) according to manufacturer's instructions (55 ° C for 0.5 min, 72 ° C for 1 min, and 95 ° C for 2.5 min). The nucleotide sequences of the specific primers for nNOSα, nNOSβ (nNOS cDNA were made according to LEE at al. and Smith at al.) (Lee, Cai et al. 1997, Smith, Merchant et al. 2009), β-MHC, ANP and GAPDH were summarized in Table 2. The PCR products were electrophoresed in a 1.5 and 2 % agarose gel at 120 V in 1X Tris-acetate-EDTA buffer and visualized using ethidium bromide.

11. Immunohistological analysis (H&E and Masson-Trichrome staining)

Rat hearts were excised while still beating and flushed with solution (in mM: NaCl 141.4, KCl 4, NaH_2PO_4 0.33, $MgCl_2$ 1,

HEPES 10, Glucose 5.5, $CaCl_2$ 1.8, Mannitol 14.5, pH of 7.4) followed by PBS (using a 20-gauge needle) and finally, fixed by using 4 % paraformaldehyde (in PBS). The hearts were dehydrated through a graded series of alcohol concentrations and then paraffin-embedded. Step-wise serial sections (5 mm thick) were taken every 75 mm from the base and stained with hematoxylin and eosin or with trichrome and examined by light microscopy. The immunostained heart tissues were imaged using a TissueFAXS (Zeiss, Leica, Nikon) with an objective of 40X.

12. Echocardiography

Transthoracic echocardiogram was performed 4 weeks after the injection of SMTC, Ang II and SMTC+Ang II or Sham procedure. Animals were placed in dorsal recumbent position under light sedation with isoflurane (3-4 % mixed with oxygen). Images were obtained by a portable echocardiographic system (Vivid Q Portable Ultrasound Machine; GE Healthcare, Pittsburgh, PA, USA) equipped with a 10-MHz transducer (10S-RS; GE Healthcare, Pittsburgh, PA, USA). Under parasternal short-axis view, M-mode cursor was positioned at the papillary muscles level, perpendicular to LV interventricular septum (IVS) and

posterior wall (PW). LV end-diastolic and end-systolic dimensions (LVEDD and LVESD) and wall thickness of PW and IVS were determined according to the leading-edge method of the American Society of Echocardiography. LV fractional shortening (FS, %) was calculated as 100 × (LVEDD − LVESD) / LVEDD, and LV ejection fraction (EF, %) was determined as 100 × ($LVEDD^3$ − $LVESD^3$) / $LVEDD^3$

13. Transmission electron microscopy (TEM)

The cardiac tissue was fixed in Karnovsky's solution (2.0 % paraformaldehyde, 2.5 % glutaraldehyde, 0.1 M Sodium cacodylate buffer). The LV septum tissue was cut into small pieces (1 mm cubes) and stained overnight in 1 % osmium tetroxide and 0.8 % potassium ferrocyanide. The following day, tissue was stained for 2 hrs in 2 % uranyl acetate and subsequently dehydrated in a series of ethanol and acetone washes. The tissue was embedded in Durcupan resin (EMD, Gibbstown, NJ, USA) and ultrathin sections (60-70 nm) were stained with lead citrate. Electron micrographs were recorded by using a JEOL 1200EX electron microscope operated at 80 kV.

14. Measurement of LV myocyte contraction and intracellular Ca^{2+} transients; myofilament Ca^{2+} sensitivity analysis

Isolated LV myocytes were superfused with a solution containing (in mM: NaCl 141.4, KCl 4, NaH_2PO_4 0.33, $MgCl_2$ 1, HEPES 10, Glucose 5.5, $CaCl_2$ 1.8, mannitol 14.5, pH 7.4 NaOH). Changes in sarcomere length and Ca^{2+} transients were measured in LV myocytes by using a video-sarcomere detection system (IonOptix Corp). For Ca^{2+} measurements, LV myocytes were pre-incubated with a Ca^{2+} indicator, acetoxymethyl ester of Fura-2 (2 μM) in perfusion solution containing 250 μM Ca^{2+} for 15 minutes at room temperature in the dark. After sedimentation, the supernatant was removed and LV myocytes were washed in perfusion solution containing 500 μM Ca^{2+} for ten minutes after which the cells were finally washed in 500 μM Ca^{2+} perfusion solution before being used. In some cells, sarcomere shortening and Fura-2 ratio were recorded simultaneously and phase-plane diagrams of Fura-2 ratio *vs.* sarcomere length was used to assess the myofilament Ca^{2+} sensitivity between the study groups. The rightward shift of the gradient of the Fura-2-

sarcomere length trajectory during late relaxation of the twitch contraction indicates reduced myofilament response to Ca^{2+}.

Measurements from at least 10 steady state contractions were averaged for each myocyte and for each stage of the experimental protocols. All experiments were carried out at 36±1 ° C and field-stimulated at 2 Hz.

15. Immunoprecipitation

LV myocytes were washed with PBS (Gibco) and lysed for 30 min on ice in lysis buffer with protease inhibitor cocktail (Roche). Cell lysates were then centrifuged at 15,000 g for 30 min at 4 ℃. The protein concentrations were determined by Bradford protein assay (Bio-Rad). The supernatants containing 500 μg of total proteins were pre-cleared with 20 μl of the protein A/G beads (Santa Cruz Biotechnology) at 4 ℃ for 30 min. Pre-cleared proteins were incubated overnight at 4 ℃ with 5 μg/ml anti-nNOS (Ab 2 - Santa Cruz Biotechnology, 200 μg/ml). 30 ml protein A/G beads were added and incubated for another 5 h to precipitate nNOS antibody. Subsequently, the beads were washed 3 times with washing buffer (0.1 % Triton X-100, 50 mM Tris-Cl pH 7.5, 150 mM NaCl, 1 mM EDTA), and the

immunoprecipitated proteins were eluted with 30 ml 2X Laemmli buffer and subjected to Western blot analysis with nNOS. Nonimmune mouse IgG (MILLIPORE) was used as a negative control.

16. Statistics

Data were expressed as means ± S.E. and n indicates the number of samples used. For all comparisons, primary cells were obtained from a minimum of three hearts per treatment group per protocol. Data were indicated as *n*. paired or unpaired Student's t-test that was used for statistical analysis. A value of $p<0.05$ was considered to be statistically significant.

Table 1. List of the primary and secondary antibodies used in the study

Antibody for immunoblotting

Primary antibody	
➢ **nNOS (Ab-1)**	Mouse monoclonal (BD Transduction Laboratories; 1:1000)
➢ **nNOS (Ab-2)**	Mouse monoclonal (Santa Cruz Biotechnology; 1:1000)
➢ **Nebulette**	Mouse monoclonal (Santa Cruz Biotechnology; 1:1000)
➢ **Myosin light chain 2v**	Rabbit monoclonal (Cell Signaling; 1:1000)
➢ **Desmin**	Rabbit polyclonal (Abcam; 1:1000)
➢ **Troponin I**	Rabbit polyclonal (Cell Signaling; 1:1000)
➢ **α-Sarcomeric actin**	Mouse monoclonal (Sigma; 1:2500)
➢ **Troponin C**	Mouse monoclonal (Abcam; 1:2500)
➢ **Tropomyosin**	Mouse monoclonal (Sigma; 1:5000)
➢ **α-Actinin**	Mouse monoclonal (Sigma; 1:2500)
➢ **cMyBPC**	Rabbit polyclonal (Dr. Sadayppan lab; 1:5000)
➢ **GAPDH**	Goat polyclonal (Santa Cruz Biotechnology; 1:1000)
➢ **Na^+-K^+ ATPase**	Mouse monoclonal (Abcam; 1:5000)
➢ **Akt Ser^{473}**	Rabbit polyclonal (Cell Signaling; 1:1000)
➢ **Akt**	Rabbit polyclonal (Cell Signaling; 1:1000)
➢ **GFP**	Rabbit polyclonal (ThermoFischer Scientific: 1:5000)
➢ **AT2R**	Goat polyclonal (Santa Cruz; 1:1000)
➢ **$AT2R^{extracellular}$**	Rabbit polyclonal (Alomone labs; 1:500)
➢ **eNOS Ser^{1179}**	Rabbit monoclonal (Cell Signaling; 1:1000)
➢ **eNOS Thr^{495}**	Rabbit monoclonal (Cell Signaling; 1:1000)
➢ **eNOS**	Mouse monoclonal (BD Transduction Laboratories; 1:1000)
➢ **nNOS**	Mouse monoclonal (BD Transduction Laboratories; 1:1000)
➢ **GAPDH**	Goat polyclonal (Santa Cruz Biotechnology; 1:1000)
➢ **Na^+-K^+ ATPase**	Mouse monoclonal (Abcam, 1:5000)

Table 2. Nucleic acid sequences of the primers used for RT-PCR experiments

Protein	Primer	Sequence	Size (bp)
nNOSα	Forward	Exon1a: 5'-AGCGGGATCCACAGCCCTGGAACT-3'	534
	Reverse	Exon 2: 5'-CCGCAGCACCTCCTCGAATC-3'	
nNOSβ	Forward	Exon1a: 5'-AGCGGGATCCACAGCCCTGGAACT-3'	548
	Reverse	Exon 6: 5'-GCGCCATAGATGAGCTCGGTG-3'	
β-MHC	Forward	5' - GTGCTCTACAATCTCAAGGAGAGG - 3'	273
	Reverse	5' - GACCCTCTTGGTGTTGACGG - 3'	
ANP	Forward	5' - AGCGAGCAGACCGATGAAG - 3'	162
	Reverse	5' - AGCCCTCAGTTTGCTTTTCA - 3'	
GAPDH	Forward	5' - GCCAAGGCTGTGGGCAAGGT - 3'	268
	Reverse	5' - GAGCAATGCCAGCCCCAGCA - 3'	

CHAPTER 1

Mechanism leading to nNOS up-regulation by angiotensin II in rat cardiac myocyte

INTRODUCTION

The renin-angiotensin system (RAS) exerts pleiotropic roles in normal cardiovascular functions and in various cardiovascular diseases. Ang II is the major active peptide that is produced locally and systematically that mediates the effects of RAS by disturbing intracellular ion homeostasis, oxidative stress and abnormal signaling pathways, consequently leading to hypertension, hypertrophy, heart failure and atherosclerosis (Unger 2002, Varagic and Frohlich 2002, Ramchandran, Takezako et al. 2006, Oyamada, Bianchi et al. 2010). The multitudinous effects of Ang II are predominantly mediated by AT1R activation of various signaling cascades including NADPH oxidase and resultant reactive oxygen species (ROS) and protein kinases trigger an array of diverse signaling pathways to promote cardiovascular pathogenesis (Heusch and Schulz 2011, Patel and Schultz 2013). On the other hand, AT2R counteracts the detrimental effects of AT1R and cardiac oxidase-derived oxidative stress and protects the heart from disease development (Jalowy, Schulz et al. 1998, Jones, Vinh et al. 2008, Padia and Carey 2013). In fact, AT2R exerts these functions by

activating protein phosphatases, protein tyrosine phosphatase and protein phosphatase 2A, and dephosphorylation of downstream effector proteins modifies their activities. Alternatively, AT2R is well established to activate nitric oxide synthase (NOS)/NO—cyclic guanosine 30, 50−monophosphate (cGMP) signaling to exert protective effects in cardiovascular system (Heusch, Post et al. 2000, Jones, Vinh et al. 2008, Padia and Carey 2013). General consensus is that eNOS is the downstream target of AT2R (Nguyen Dinh Cat, Montezano et al. 2013, Padia and Carey 2013). However, despite nNOS is the predominant NOS that regulates cardiac contractility and intracellular Ca^{2+} homeostasis in cardiac myocytes, the involvement of nNOS in AT2R−mediated downstream signaling is unknown. In this chapter, we examined upregulation mechanisms mediating Ang II−stimulation of nNOS in LV myocytes from healthy rats.

RESULTS

1-1. Ang II increases nNOS protein expression by ROS-dependent AT2R translocation to plasma membrane.

Intracellular ROS are upstream regulators of the transcription of proteins and are associated with cardiac NOS protein expression and activity (Cai, Li et al. 2002, Sartoretto, Kalwa et al. 2011). Therefore, I tested whether intracellular ROS subsequent to AT1R activation is involved in Ang II-upregulation of nNOS. Fig. 3 shows that Ang II (1 μM, 3 hrs) increased nNOS protein expression. Furthermore, pre-treatment of LV myocytes with apocynin, tiron or H_2O_2 catalase-polyethylene glycol (PEG-catalase, 352 Units/ml) abolished Ang II-induced increases in nNOS protein expression (p<0.001 between Ctr and Ang II, n=10; p=0.002 between Ang II and Ang II+apocynin, n=6; p<0.001 between Ang II and Ang II+tiron, n=6; p=0.03 between Ang II and Ang II+PEG-catalase, n=5, Fig. 3). Involvement of both pathogenic AT1R/ROS and counterbalancing AT2R in Ang II-stimulation of nNOS suggest that there may be crosstalk between Ang II receptors. Therefore, using biotinylation and western blotting analysis of the plasma

membrane of LV myocytes, we examined membrane expressions of the Ang II receptors following Ang II treatment. AT2R in biotinylated membrane fraction was increased with Ang II (at 30 min, p=0.02 between Ctr and Ang II, n=9, Fig. 4). Intriguingly, pre-treatment of LV myocytes with losartan blocked Ang II-induced AT2R translocation to plasma membrane (AT2R density in biotinylated membrane fraction was reduced, p=0.01 between Ang II and Ang II+losartan, n=6, Fig. 4). Similarly, apocynin or tiron pre-treatment blocked Ang II-induced AT2R translocation to the plasma membrane of LV myocytes (p=0.02 between Ang II and Ang II+apocynin, n=6; p=0.04 between Ang II and Ang II+tiron, n=6, Fig. 4). These results clearly suggested that nNOS was increased by ROS-dependent AT2R translocation to plasma membrane after treatment with Ang II for 3 hrs in LV myocytes (Fig. 3 and 4). Previously, these results were referred in the thesis of master's degree.

1-2. eNOS is activated by Ang II and intracellular ROS.

Next, I detected whether eNOS activity is also regulated by Ang II and if so, how does eNOS affect nNOS protein expression. The result showed that eNOS Ser^{1177} was increased by Ang II

whereas eNOS Thr^{495} was reduced from minutes of application (p=0.03 and p<0.001 between Ctr and Ang II 30 min, respectively, n=4, Fig. 5A), and eNOS dimer form was not changed by Ang II treatment (Fig. 5B). It is known that Akt phosphorylation is one of the upstream regulators of eNOS. Similarly, Fig. 6 showed that Ang II time-dependently increased Akt phosphorylation in cardiac myocytes (p=0.01 between Ctr and Ang II 30 min, n=3). Furthermore, apocynin pre-treatment decreased eNOS Ser^{1177} phosphorylation and blocked eNOS Thr^{495} dephosphorylations by Ang II (p=0.006 and p=0.63 between Ctr and Ang II 30 min, respectively, n=4, Fig. 7), suggesting that increased intracellular ROS is responsible for Ang II-regulation of eNOS.

1-3. Pivotal role of eNOS in Ang II-induced AT2R translocation and nNOS protein expression

I tested the hypothesis that eNOS mediates Ang II-stimulation of cardiac nNOS. Indeed, L-NAME pre-treatment abolished Ang II-induced nNOS protein expression (p=0.03 between Ang II and L-NAME+Ang II, n=4, Fig. 8A). To confirm the role of eNOS in Ang II-induced nNOS protein expression, I detected the

effect of Ang II on nNOS protein expression in LV myocytes from $eNOS^{+/+}$ and $eNOS^{-/-}$ mice. As shown in Fig. 8B, Ang II increased nNOS protein expression in $eNOS^{+/+}$ LV myocytes (p=0.01, n=4). However, nNOS protein expression was unaffected by Ang II in $eNOS^{-/-}$ LV myocytes (p=0.95, n=4, Fig. 8B). Therefore, I examined the role of eNOS in Ang II-induced and eNOS-mediated AT2R translocation to plasma membrane and nNOS protein expression. AT2R density in biotinylated membrane fractions were significantly reduced in L-NAME pre-treated LV myocytes (p=0.02 between Ang II and L-NAME+Ang II, n=5, Fig. 9A). In addition, AT2R translocation to plasma membrane was observed with immunocytochemistry in non-permeabilized primary LV myocytes. Fluorescent intensity for extracellular membrane-specific AT2R antibody was significantly increased after Ang II or SNP treatment (10 μM, 30 min) (Fig. 9B). However, Ang II failed to induce surface expression of AT2R in L-NAME pre-treated LV myocytes.

1-4. S-nitrosation of AT2R by NO

Increased eNOS production of NO may prompt AT2R translocation *via* S-nitrosation of AT2R. Therefore, I aimed to

determine whether AT2R could be S-nitrosated by NO increment. Ang II treatment did not affect S-nitrosation of AT2R, possibly due to high reducing environment in LV myocytes. However, SNP significantly increased S-nitrosation of AT2R (p=0.02, n=3, Fig. 10A). Conversely, pre-incubation of LV myocytes with a strong reducing agent, DTT (1 μM), abolished Ang II increase of nNOS protein expression (p=0.018, n=5, Fig. 10B).

1-5. C-terminal cysteine 349 of AT2R is essential in membrane trafficking.

Using site-directed mutagenesis on DNA construct of GFP conjugated AT2R, I went on and analyzed potential target of NO in AT2R that may convey membrane trafficking. I determined to test the 4 cysteine residues on the intracellular region of AT2R due to the bioavailable environment of NO in the cytosol (Fig. 11). Wild type and cysteine 70, 71, 319 and 349 mutations to alanine were transfected in HEK293T cells; NO-dependent membrane trafficking of AT2R was determined using surface biotinylation and immunocytochemistry. As shown in Fig. 12, surface to total AT2R ratio was significantly increased by SNP

(10 μM, 30 min) in wild type AT2R (p=0.004 between Ctr and SNP in AT2R-WT, n=3). Similar increases in surface to total AT2R ratios by SNP were observed in C70A, C71A, C319A mutants (p=0.02, between Ctr and SNP in AT2R-C70A; p=0.03, between Ctr and SNP in AT2R-C71A; p=0.01, between Ctr and SNP in AT2R-C319A, respectively, n=3, Fig. 12). Unexpectedly, C349A mutation increased AT2R translocation to plasma membrane before SNP treatment (p=0.005 between AT2R-WT and AT2R-C349A, n=3, Fig. 12). And this increase was sustained by SNP treatment in C349A transfected cells. In concordance with surface biotinylation data, AT2R-C349A expression was increased in plasma membrane before SNP treatment and remained to the same level after SNP treatment (Fig. 13). In contrast, AT2R translocation to plasma membrane was increased by SNP in AT2R-WT, C70A, C71A, C319A transfected cell (Fig. 13). These results suggest that cysteine 349 of AT2R is a key regulatory site for AT2R translocation to the plasma membrane. Furthermore, AT2R translocation by eNOS activation is important in mediating Ang II-induced increase in nNOS protein expression in rat LV myocytes.

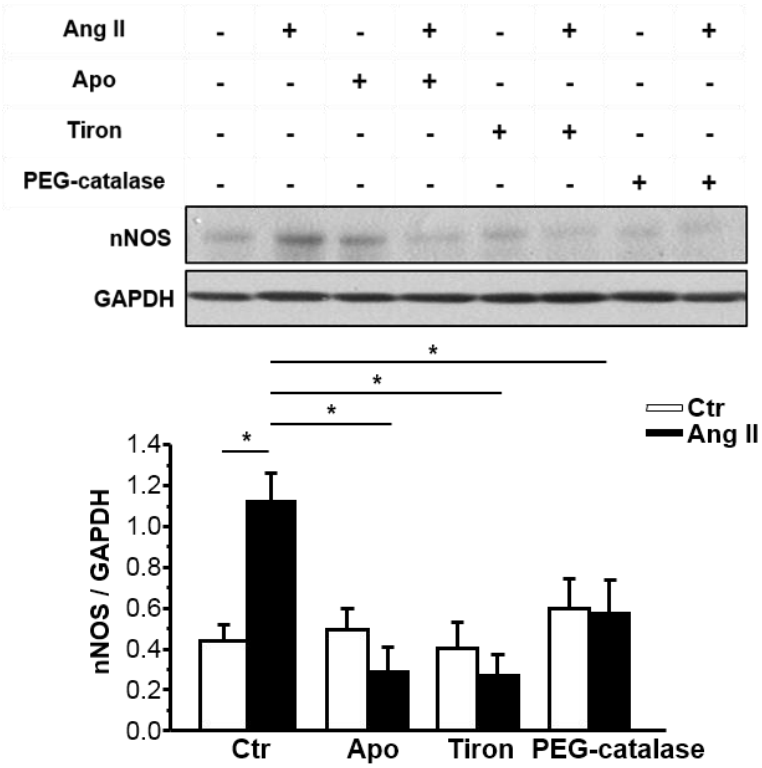

Figure 3. Inhibition of NADPH oxidase activity and ROS production prevented Ang II-induced nNOS protein expression.

Ang II (1 μM) was treated for 3 hrs in isolated LV myocytes. Apocynin (Apo, 100 μM), tiron (1 mM), PEG-catalase (352 units/ml) pre-treatment (30 min) abolished nNOS protein expression in Ang II-incubated LV myocytes. GAPDH was used as a loading control.

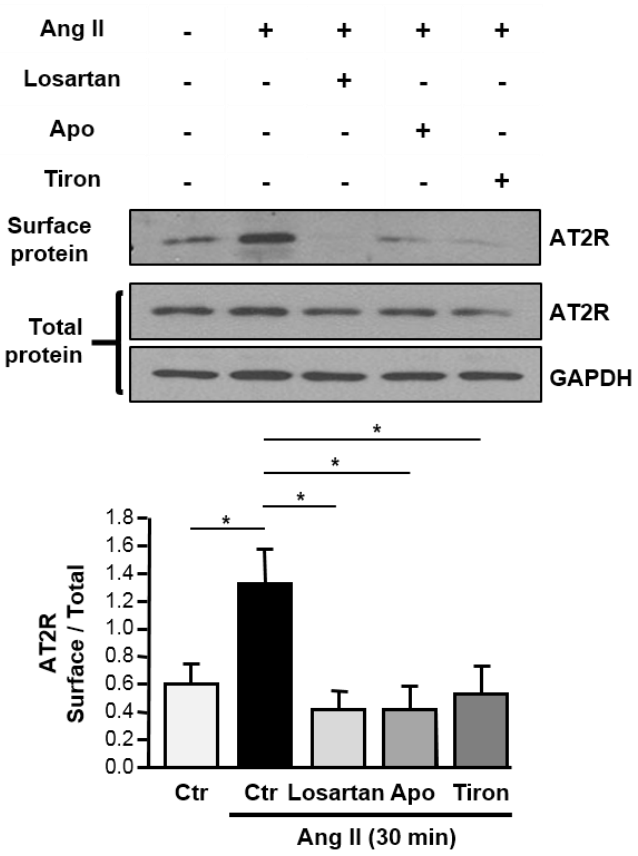

Figure 4. AT1R-dependent activation of NADPH oxidase and ROS induced AT2R translocation to plasma membrane in Ang II-treatmented LV myocytes.

Images of the immunoblotting (upper) and the mean ratio of AT2R (surface/total) (lower). Losartan (1 μM), Apocynin (Apo, 100 μM) and Tiron (1 mM) pre-treatment in LV myocytes prevented Ang II-stimulation of AT2R translocation to plasma membrane. GAPDH was used as a loading control.

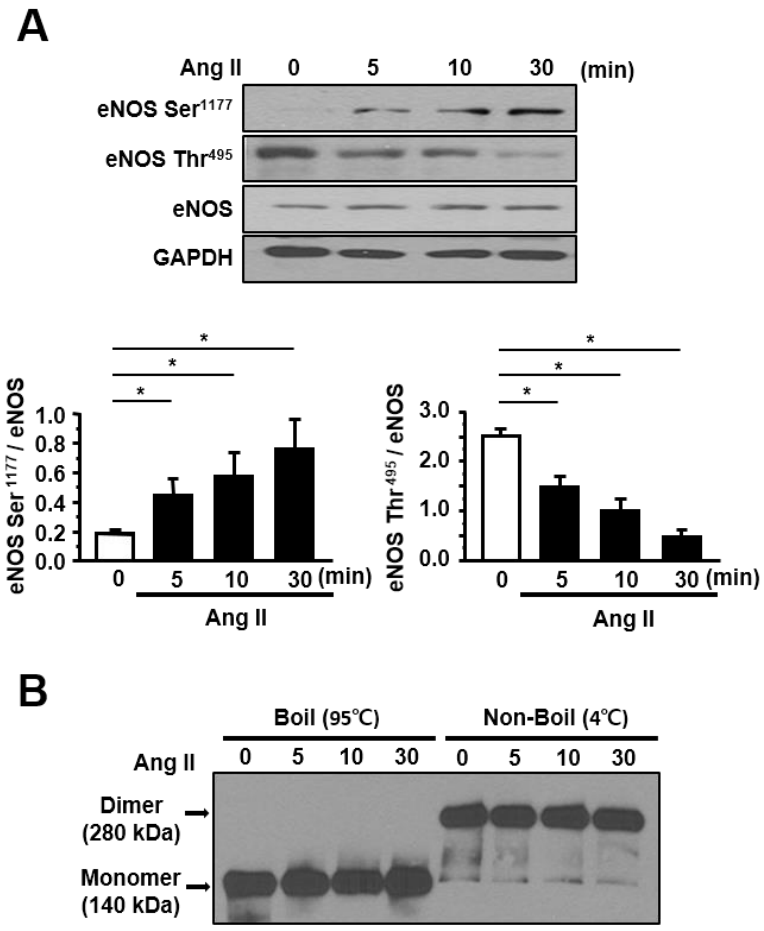

Figure 5. eNOS Ser^{1177} and eNOS Thr^{495} were inversely regulated by Ang II in LV myocytes.

(A) eNOS Ser^{1177} and eNOS Thr^{495} phosphorylations in Ang II-treated LV myocytes (5, 10, 20, 30 min). Representative immunoblottings and averaged ratios for eNOS Ser^{1177}/eNOS and eNOS Thr^{495}/eNOS. (B) eNOS dimer protein was detected as a non-boiled sample (280 kDa). All eNOS monomer protein was detecetd as a boiling at 95 ℃ (140 kDa).

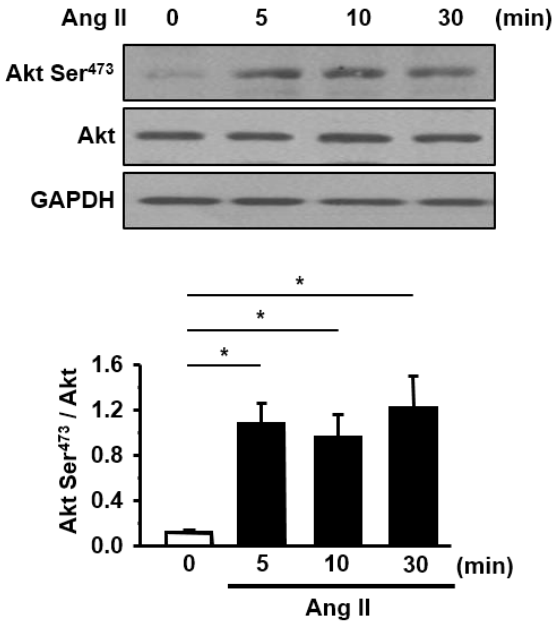

Figure 6. Akt Ser^{473} was increased by Ang II in LV myocytes.

Total and phosphorylated Akt (Akt Ser^{473}) in response to Ang II (5, 10, 30 min) were detected in isolated LV myocytes.

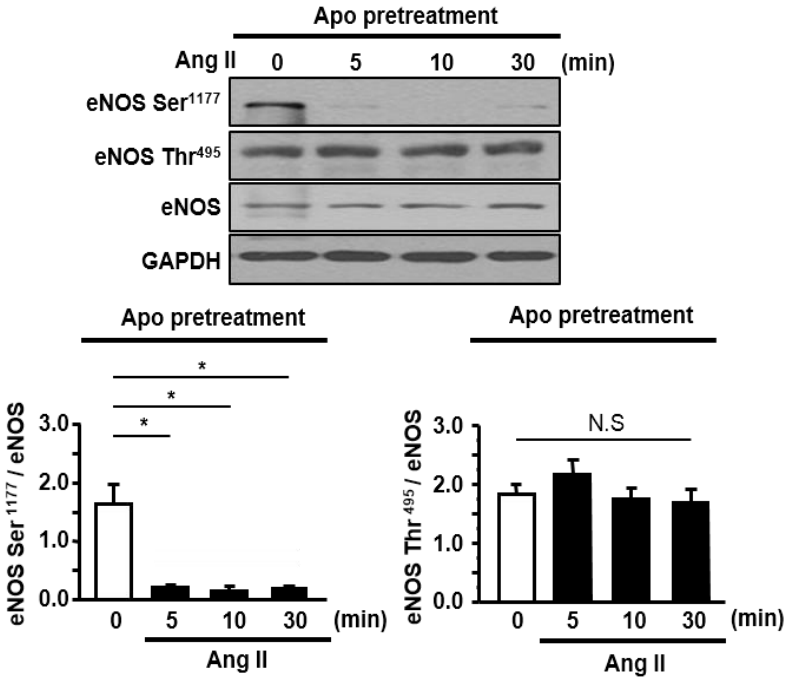

Figure 7. Inhibition of NADPH oxidase decreased eNOS Ser^{1177} without an effect on eNOS Thr^{495}.

eNOS Ser^{1177} and eNOS Thr^{495} were immunoblotted after apocynin pretreatment (30 min) in Ang II-treated LV myocytes (5, 10, 20, 30 min). Representative immunoblottings (upper) and averaged ratios for eNOS Ser^{1177}/eNOS and eNOS Thr^{495}/eNOS (lower).

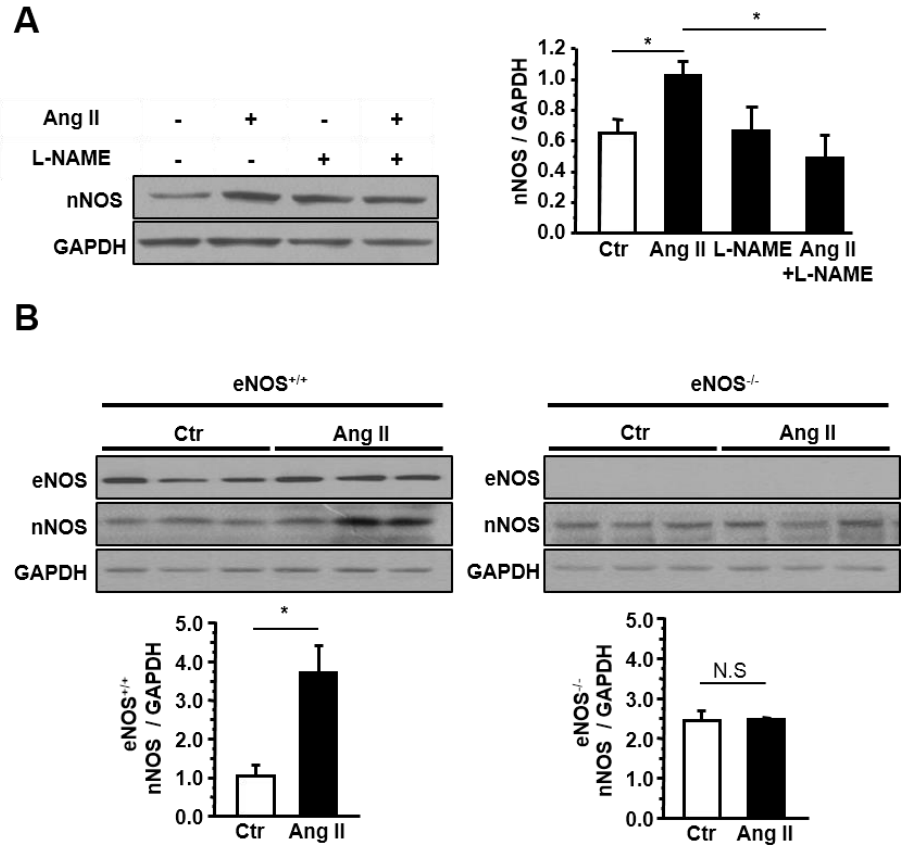

Figure 8. eNOS inhibition or gene deletion abolished Ang II-induced nNOS protein expression.

(A) L-NAME (1 mM) pre-treatment blocked Ang II stimulation of nNOS protein expression. (B) Isolated LV myocytes in $eNOS^{+/+}$ and $eNOS^{-/-}$ mice were treated with Ang II (1 μM) for 3 hrs. nNOS protein expression was increased by Ang II in $eNOS^{+/+}$ but not in $eNOS^{-/-}$ LV myocytes.

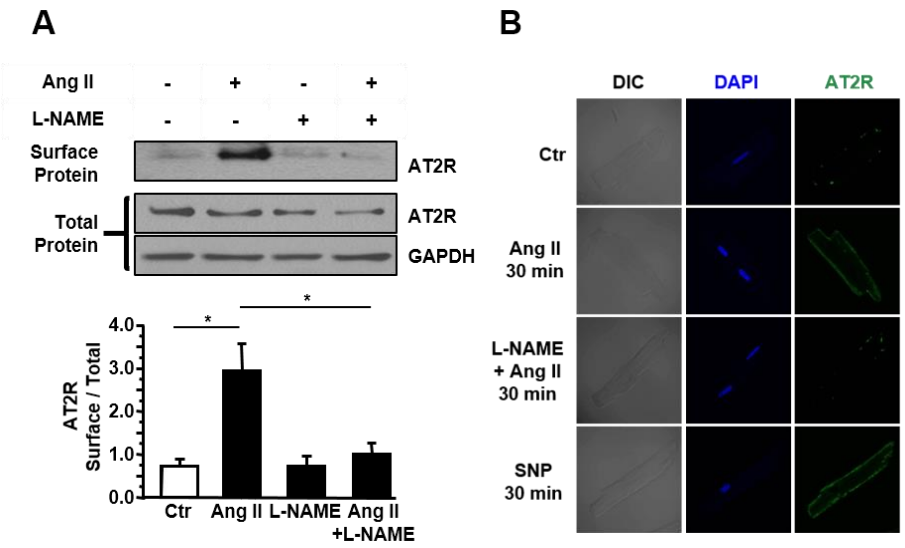

Figure 9. AT2R translocation to plasma membrane in Ang II–treated LV myocytes was prevented by inhibition of eNOS.

(A) Surface biotinylation of AT2R was conducted in Ang II (1 μM) and Ang II+L–NAME (1 mM)–treated LV myocytes (30 min). GAPDH was used as a loading control in total protein quantification. (B) Ang II and SNP (30 min)–dependent AT2R translocation to plasma membrane was detected by immunocytochemistry with an antibody detecting extracellular AT2R (green) in non–permeabilized LV myocytes.

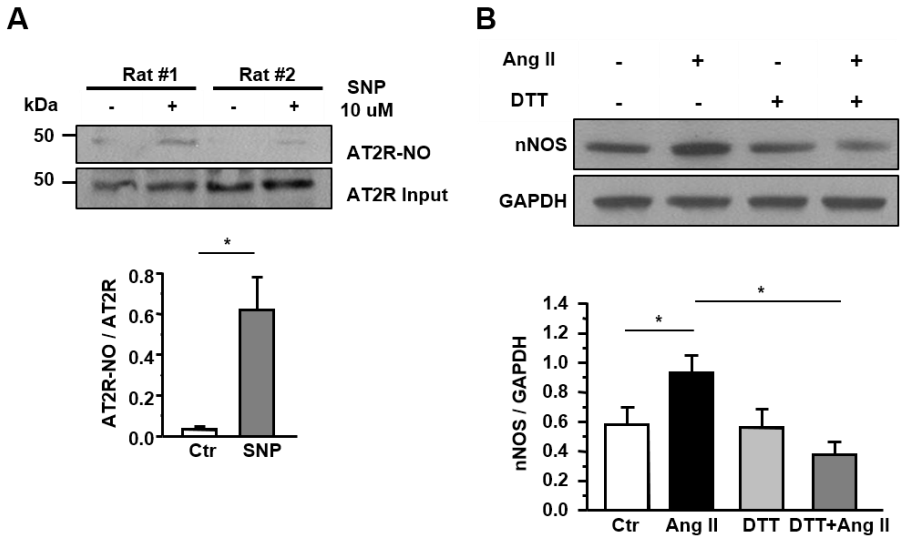

Figure 10. S-nitrosation of AT2R is necessary for Ang II-stimulation of nNOS protein expression.

(A) Representative immunoblots and mean ratios of AT2R S-nitrosation (relative to total AT2R) in the presence and absence of SNP (10 μM). S-nitrosated AT2R was increased by SNP. (B) DTT pretreatment (1 mM, 30 min) abolished Ang II-induction of nNOS protein expression.

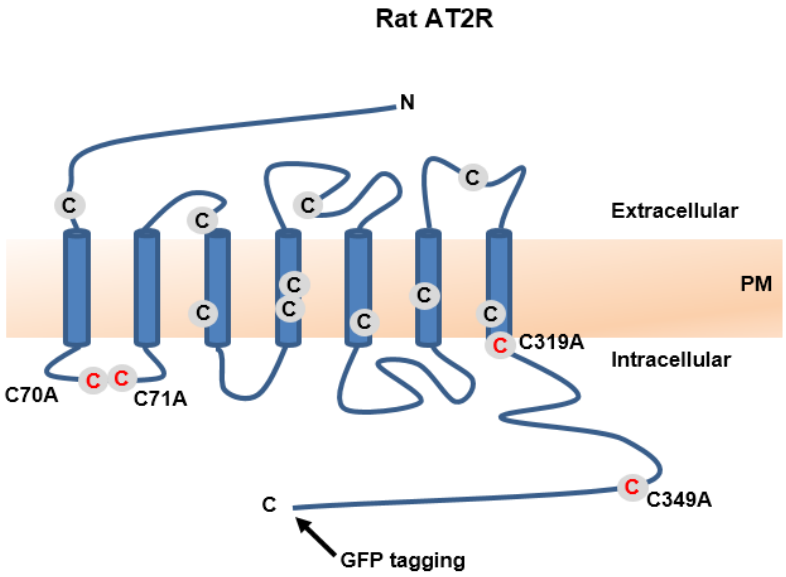

Figure 11. The structure of AT2R and the cysteine residues in extracellular, transmembrane and cytosolic domains

The AT2R protein has four cysteine residues in intracellular region. The arrowhead indicates the position where GFP was inserted to make GFP-tagged AT2R (AT2R-GFP). The targeted mutations of cysteine were marked in red.

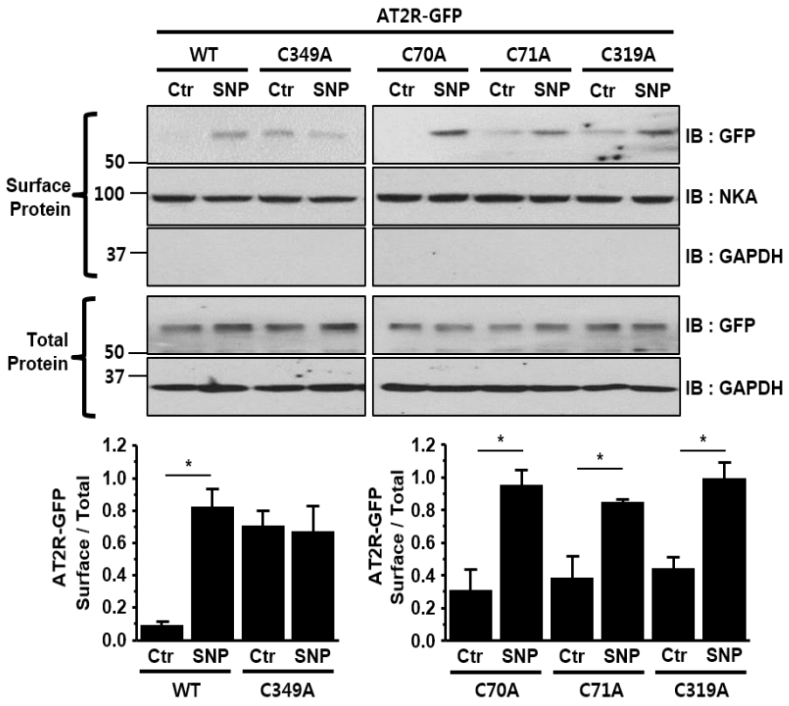

Figure 12. Cysteine 349 of AT2R is critical for the translocation of AT2R to plasma membrane – determined by surface biotinylation.

HEK293T cells were transfected with AT2R-WT, C70A, C71A, C319A, C349A mutants, respectively. Each mutant was treated with SNP (10 μM). Quantification of the mutants was identified by GFP protein. Na^+-K^+ ATPase (NKA) was detected as a loading control for surface fraction. Bar graph represents the ratio of surface to total GFP protein.

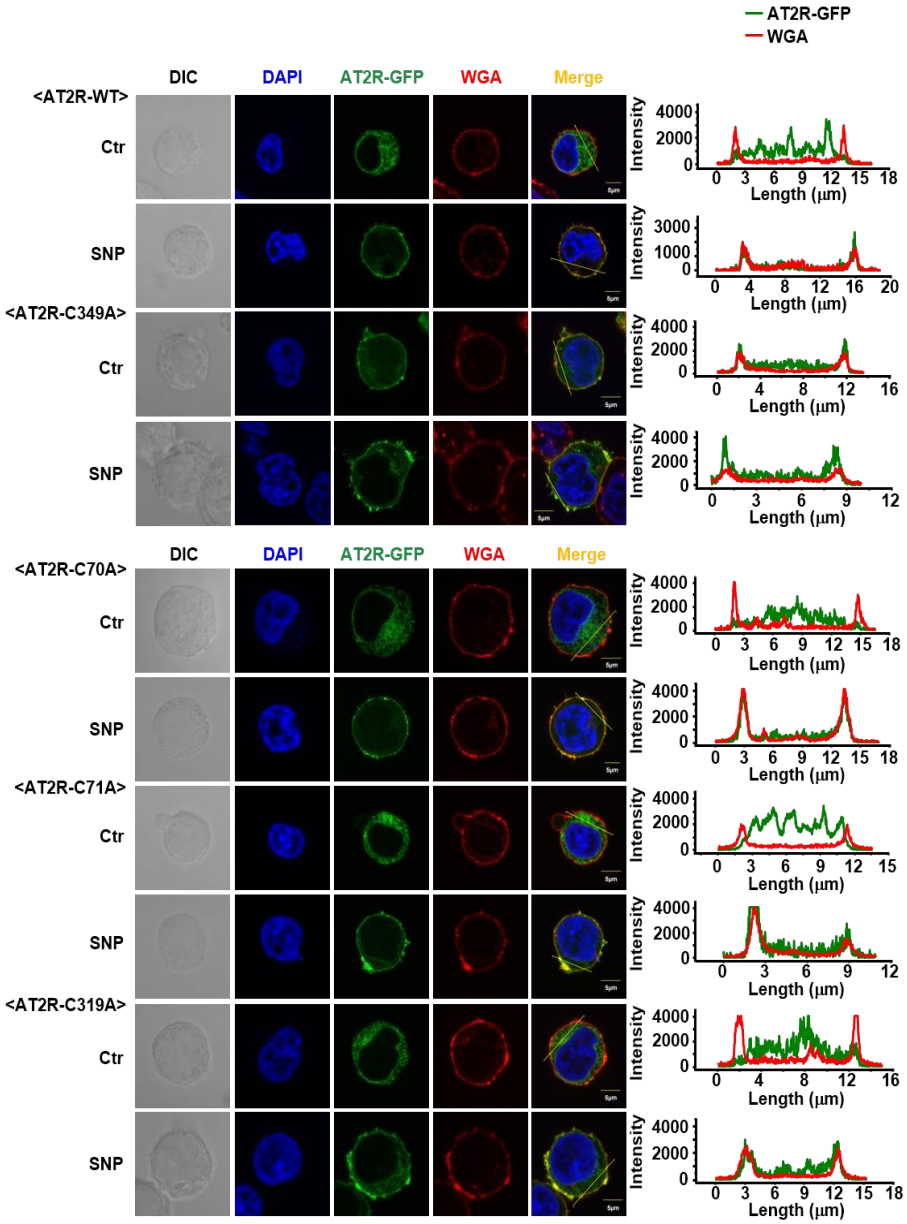
AT2R-GFP
WGA
DIC
DAPI
AT2R-GFP
WGA
Merge
<AT2R-WT>
Ctr
SNP
<AT2R-C349A>
Ctr
SNP
<AT2R-C70A>
Ctr
SNP
<AT2R-C71A>
Ctr
SNP
<AT2R-C319A>
Ctr
SNP
Intensity
Length (μm)

Figure 13. Cysteine 349 of AT2R is critical for the translocation of AT2R to plasma membrane – determined by immunocytochemistry in confocal microscopy.

Expression of AT2R-GFP (green) was localized in the cytoplasm in HEK293T cell. The surface expression of AT2R-GFP was identified by WGA (red). The right panel showed the intensities of AT2R-GFP (green) and WGA (red) on yellowed dashed lines of the images. Scale bar 5 μm.

DISCUSSION

In the present study, I demonstrate that (1) Ang II increases nNOS protein expression *via* AT1R–ROS–dependent AT2R translocation to plasma membrane. (2) eNOS is activated by Ang II and mediates Ang II–stimulation of AT2R translocation to plasma membrane; (3) eNOS activation is important in Ang II stimulation of nNOS protein expression in cardiac myocytes; (4) Furthermore, I showed direct evidence that AT2R can be S–nitrosated by NO; (5) C–terminal cysteine 349 of AT2R is a critical site for the trafficking of AT2R to the plasma membrane of cardiac myocyte. To my knowledge, this is the first study to reveal interplays between eNOS activation—nNOS expression in cardiac myocytes. Schematic diagram of the cascade is shown in Fig. 14.

Functional involvement of Ang II receptors in the regulation of NOSs

AT1R has been implicated in the activation of constitutive NOS in cardiovascular system. For example, using transgenic mice model that expresses constitutively active AT1R in endothelial

cells, Ang II increased eNOS activity (Jalowy, Schulz et al. 1998) and led to hypotension in these mice (Ramchandran, Takezako et al. 2006). Similar increase in eNOS protein expression by Ang II was shown in endothelial cells in vitro (Cai, Li et al. 2002) or in the myocardium (Tambascia, Fonseca et al. 2001, Ritter, Schuh et al. 2003). Conversely, losartan (AT1R receptor antagonist) reduced NO production in cardiac myocytes and impaired NO bioavailability was partially responsible for larger infarct size following ischemia (Huisamen, Perel et al. 2011). The relationship between AT2R and nNOS protein expression has been discussed previously. For example, AT2R agonist, C21, treatment significantly upregulated nNOS expression in the paraventricular hypothalamic nucleus (PVN) and rostral ventrolateral medulla (RVLM) and negatively regulated sympathetic outflow and improved baroreflex sensitivity via a nNOS dependent mechanism (Gao, Zhang et al. 2011, Gao, Zucker et al. 2014). Conversely, inhibition of AT2R abolishes relaxin-induced nNOS protein expression and phosphorylation, and subsequently prevents anti-fibrotic actions of relaxin (Chow, Kocan et al. 2014). In addition, nNOS protein expression has been shown to be unaffected in the infarcted myocardium from

AT2R-deficient mice (Brede, Roell et al. 2003), in contrast to the upregulation of nNOS protein in failing myocardium (Bendall, Damy et al. 2004, Damy, Ratajczak et al. 2004). In the present study, I also show that eNOS activity is increased by Ang II (30 min) and eNOS-derived NO is necessary for AT2R trafficking to increase nNOS protein expression (eNOS begets nNOS). I am not stating that eNOS is the exclusive mechanism to induce nNOS in cardiac myocytes. In fact, nNOS compensates for reduced NO bioavailability in the absence of eNOS in the cardiovasculature under stress (Huang, Sun et al. 2002, Damy, Ratajczak et al. 2004, Copp, Hirai et al. 2012). eNOS may become a key player in AT1R-NADPH oxidase-AT2R axis due to its influences on AT2R translocation and activation, despite the fact that eNOS-regulation of myocardial contraction is trivial both under basal conditions and with β-adrenergic stimulation (Post, Schulz et al. 2001, Zhang and Casadei 2012). In essence, eNOS is activated by Ang II (mediated by ROS) and is necessary as an early signal to mediate Ang II-stimulation of nNOS. Notably, Ang II progressively increased eNOS Ser^{1177} but reduced eNOS Thr^{495} (Fig. 5). One possibility is that Ang II causes PP2A activation with time (downstream of AT2R) and dephosphorylates eNOS

Thr^{495}, whereas eNOS Ser^{1177} is more sensitive to ROS-activating protein kinases (e.g., Akt). On the other hand, apocynin without Ang II significantly increased eNOS Ser^{1177} (Fig. 6). Since PP2A activity is known to be suppressed by antioxidants (e.g., ascorbate), followed by enhanced AMPK-dependent eNOS Ser^{1177} (Ladurner, Schmitt et al. 2012), eNOS Ser^{1177} can be actively regulated by PP2A under basal conditions.

S-nitrosation of AT2R

Furthermore, I have demonstrated NO-dependent S-nitrosation of AT2R in LV myocytes. This effect was observed in primary LV myocytes only with SNP but not by Ang II. The lack of response of Ang II does not exclude eNOS-dependent S-nitrosation of AT2R in primary cardiac myocytes since it may occur at local compartments and is difficult to detect in myocyte lysates where NO scavengers are abundant; however, this remains elusive and may require more sensitive measurement to pinpoint the regulation. To further explore the cysteine residues in AT2R those could be responsible for NO-dependent AT2R translocation, I tested site-directed mutagenesis of DNA constructs of AT2R, conjugated with GFP. Wild type AT2R failed

to translocate to the plasma membrane in response to NO and AT2R ⊿7 (7 aa deletions in C terminus) (consistent with Dr. Wu's results (Zhang, Dong et al. 2011), data not shown). Among the four alanine to cysteine mutations (C70, 71, 319 and 349), only C349A exhibited a "gain of function mutation" and induced AT2R translocation to plasma membrane. These results show the requirement of C349 in the regulation, although the functional significance of its S-nitrosation remains clarified. One possibility is that S-nitrosation of AT2R is the prerequisite for transferring NO to adjacent target (e.g., transnitrosylation) that accomplishes AT2R translocation. The detailed regulatory mechanisms of cysteine residues of AT2R in the presence of RNS or ROS and their functional relevance in the myocardium remain to be determined.

Taken together, I revealed that AT1R-NADPH oxidase-eNOS-S-nitrosation of AT2R axis links Ang II-stimulation of nNOS protein expression in cardiac myocyte. This novel pathway may be used to design a better therapeutic regimen to improve the effectiveness of RAS-related drugs for patients with cardiovascular diseases.

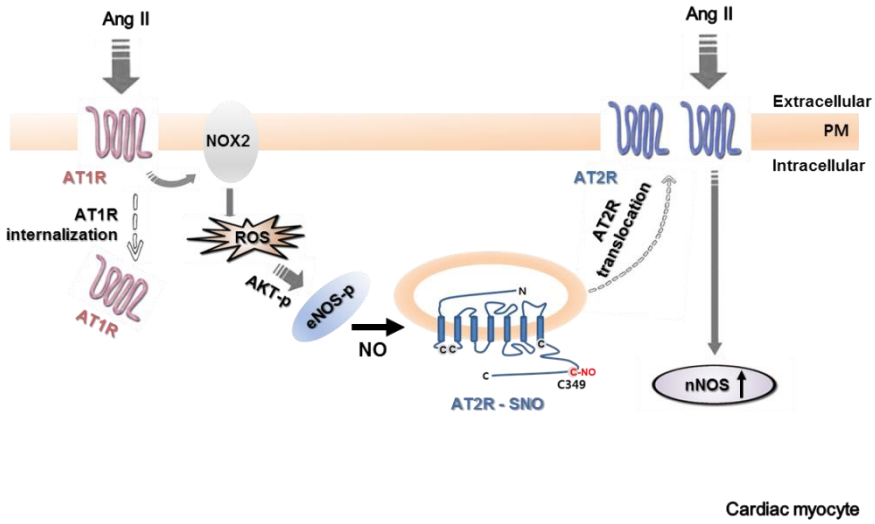

Figure 14. Schematic diagram illustrating the mechanisms of Ang II-upregulation of nNOS protein in cardiac myocytes.

Ang II stimulates AT1R in cardiomyocyte and quickly internalized, leading to activation of cardiac oxidases such as NADPH oxidase. Intracellular ROS, in turn, activates Akt and phosphorylates endogenous eNOS to activate the enzyme. Subsequently, S-nitrosation of AT2R near cysteine 349 residue contributes to AT2R translocation to the plasma membrane and was stimulated by Ang II. This leads to a rise in nNOS protein and NO generation.

-There are some parts of the contents belong to the Master's thesis

CHAPTER 2

Mechanism of nNOS-mediated cardiac protection in Ang II -induced hypertensive rat

INTRODUCTION

Among five splicing variants of nNOS (nNOSα, nNOSμ, nNOSβ, nNOSγ, nNOS −2), nNOSα, nNOSμ, and nNOSβ show the property of transferring electron from oxygenase to reductase domain (Brenman, Chao et al. 1996). nNOSα and nNOSμ (interact with other proteins in N−terminal of *via* the PDZ binding motif), are involved in the functional regulation of the binding protein through the production of NO in cardiac muscle. Under some circumstances, high concentrations of the NO scavenger such as myoglobin and glutathione in cardiac muscle may affect the efficiency of NO (Flogel, Merx et al. 2001). In the myocardium, nNOSα/μ is known to affect the activity of Ca^{2+}−regulated channel and intracellular proteins in the SR through NO−regulated posttranslational modification of target proteins (e.g phosphorylation or S−nitrosation). On the other hand, nNOSβ, which is an alternative splice variant that produces NO has been presented to exert diverse effects in the tissues other than myocardium (Hurt, Sezen et al. 2006, Bernardo, Weeks et al. 2010, Percival, Anderson et al. 2010, Cunningham, Sasser et al. 2013). However, the presence or absence of nNOSβ and its

molecular function in the myocardium was so far unidentified in healthy and diseased hearts.

As mentioned in the general introduction, pathological stimuli those cause pressure-overload, produces wall stress which results in concentric hypertrophy (Bernardo, Weeks et al. 2010, Katholi and Couri 2011). Therefore, I infused Ang II through osmotic mini-pump insertion in rats for 4 weeks to produce hypertension model (Jin, Jang et al. 2013). Together with Ang II, SMTC-containing osmotic pump was also infused to inhibit nNOS *in vivo*. Therefore, in this chapter, I aimed to examine that 1) What is the role of nNOS in myofilament structure and function in LV myocytes from normal and hypertensive rats? 2) Whether nNOSβ is functionally expressed in LV myocytes and exerts functions that is different from nNOSα/μ?

RESULTS

PART 1

Chronic inhibition of nNOS *in vivo* exacerbates cardiac hypertrophy and fibrosis in Ang II–induced hypertensive rat.

As shown in Fig. 15, I generated four groups of rats: Sham, SMTC, Ang II and SMTC+Ang II (Fig. 15). Blood pressure and heart rate were measured every 2 days for 4 weeks. At 4th week, both systolic and diastolic blood pressure were increased in Ang II (n=21) and in SMTC+Ang II (n=12) compared to those in Sham or SMTC (Figure 16A and B) and SMTC+Ang II compared to Ang II. Heart rate was lower in Ang II and in SMTC+Ang II compared with Sham and SMTC (Fig. 16C). These results demonstrate that Ang II infusion in rats induces hypertension. In addition, nNOS inhibition increases blood pressure further.

Next, I examined whether nNOS inhibition in hypertension induces morphological changes in the myocardium. Histological staining of longitudinal section of the hearts revealed substantial thickening of the LV wall and septum and a smaller LV cavity in SMTC+Ang II compared to those in Sham, SMTC and Ang II (Fig.

17A). In line with the findings, mRNA expressions of ANP and β-MHC (known as early hypertrophic gene markers) were both elevated in LV myocytes from Ang II and SMTC+Ang II (Fig. 17B). In Masson-trichrome staining, I also observed multiple regions of focal replacement fibrosis in the heart from SMTC+Ang II, but not in SMTC or Ang II (Fig. 18). Likewise, morphological and molecular examination revealed LV concentric hypertrophy in hypertension with nNOS inhibition.

Structural and functional remodeling of LV in SMTC+Ang II was analyzed further using echocardiography. The thickness of LV septum was significantly increased in SMTC+Ang II (μm: IVSd was 0.18±0.01 in Sham, 0.18±0.001 in SMTC, 0.17±0.003 in Ang II, 0.21±0.006 in SMTC+Ang II, p=0.003, n=7, between Ang II and SMTC+Ang II). Similarly, posterior wall thickness was increased in SMTC+Ang II (μm: LVPWd was 0.18±0.01 in Sham, 0.18±0.001 in Ang II, 0.18±0.004 in SMTC, 0.21±0.006 in SMTC+Ang II, p=0.005, n=7, between Ang II and SMTC+Ang II). However, end-diastolic dimension of LV was reduced in SMTC+Ang II (μm: LVIDd was 0.85±0.05 in Sham, 0.86±0.03 in SMTC, 0.85±0.05 in Ang II, 0.77±0.05 in SMTC+Ang II, p=0.018, n=7, between Ang II and SMTC+Ang

II) (Fig. 19B, C and D). Functionally, ejection fraction (LVEF) and fractional shortening (LVFS) were significantly increased in SMTC+Ang II (%: LVEF was 71.32±2.79 in Sham, 61.26±2.84 in SMTC, 67.6±2.11 in Ang II, 77.74±2.32 in SMTC+Ang II, p=0.007, n=7, between Ang II and SMTC+Ang II; LVFS was 34.58±2.55 in Sham, 29.43±1.40 in SMTC, 34.48±1.61 in Ang II, 42.71±1.74 in SMTC+Ang II, p=0.004, n=7, between Ang II and SMTC+Ang II) (Fig. 19E and F). These results demonstrate the structural and functional remodeling of LV in hypertension with nNOS inhibition, exhibiting hypertrophic cardiomyopathy phenotype.

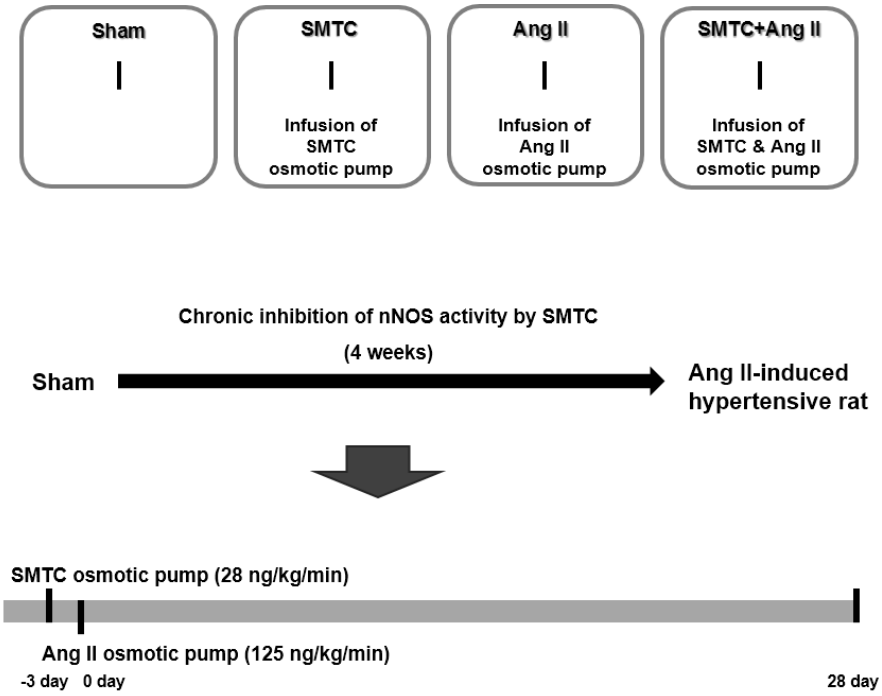

Figure 15. Flow chart of the experimental design: establishment of hypertension and nNOS inhibition in Sham and hypertensive rat models

Ang II (125 ng/kg/min) was infused through osmotic minipump for 4 weeks to produce hypertension model in rats. A specific inhibitor of nNOS, SMTC (28 ng/kg/min), was infused without and with Ang II for 4 weeks to inhibit nNOS activity systematically. Blood pressure and heart rate were monitored every 2 days.

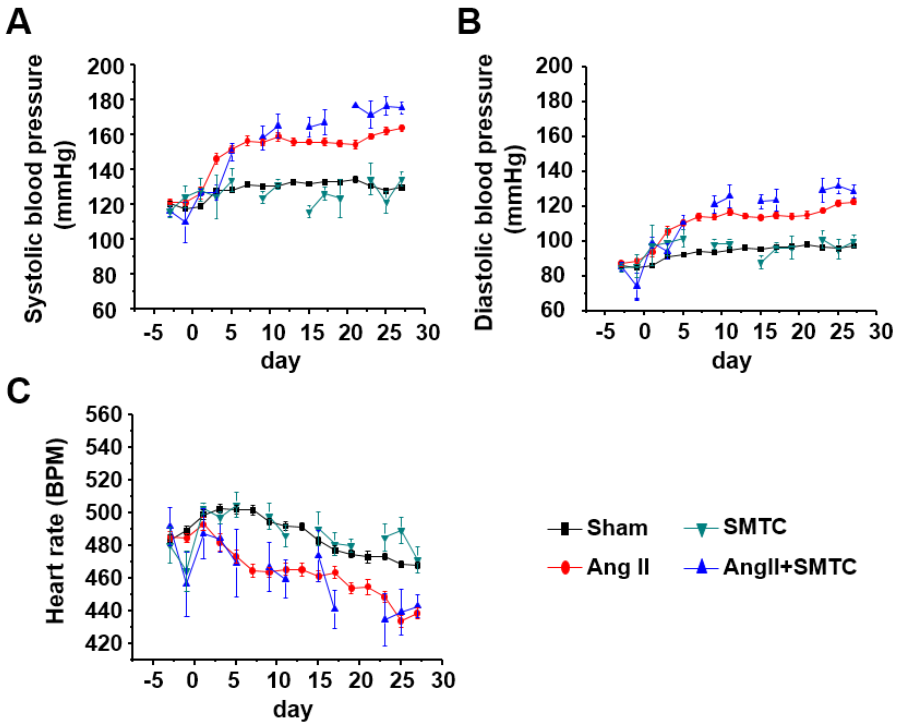

Figure 16. Changes of blood pressure and heart rate in Sham, SMTC, Ang II and SMTC+Ang II

(A, B) Mean systolic (A) and diastolic (B) blood pressure measurements over 4-week period. Both systolic and diastolic pressures were significantly increased in Ang II compared to those in Sham. SMTC increased blood pressure further in Ang II. (C) The mean heart rate was reduced in Ang II and in SMTC+Ang II.

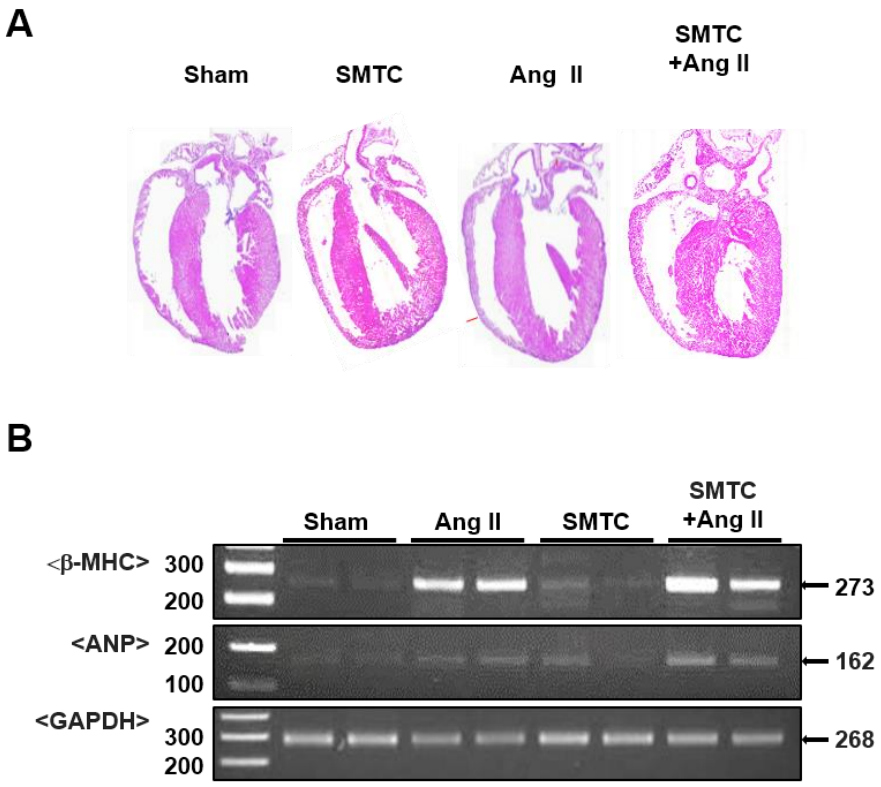

Figure 17. Histological demonstration of concentric hypertrophy in the LV of Sham, SMTC, Ang II and SMTC+Ang II

(A) H&E staining of the heart sections in Sham, SMTC, Ang II and SMTC+Ang II. LV wall thickness was significantly increased but LV chamber was reduced in SMTC+Ang II compared to the other 3 groups. (B) Expressions of β-MHC and ANP mRNA in isolated LV myocytes. β-MHC and ANP mRNA were increased in Ang II and in SMTC+Ang II. GAPDH was used as the loading control.

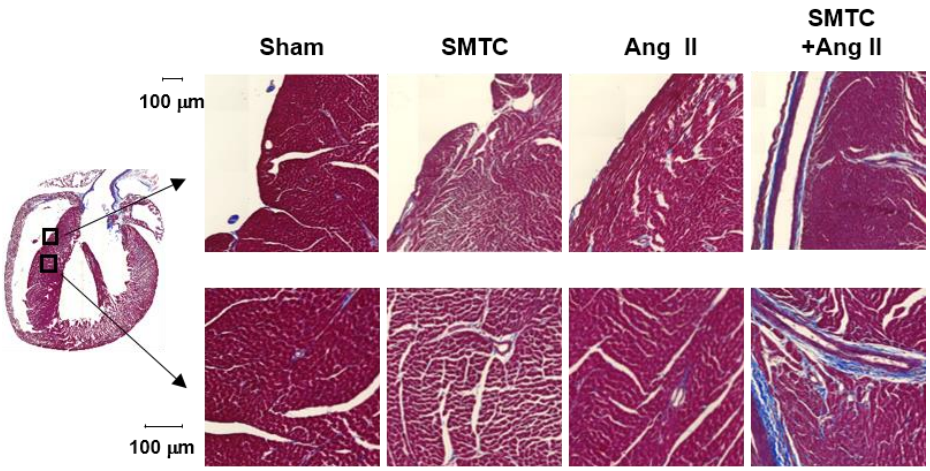

Figure 18. Histological demonstration of the fibrosis in the LV of Sham, SMTC, Ang II and SMTC+Ang II

Masson's trichrome staining in LV myocardium of Sham, SMTC, Ang II and SMTC+Ang II. Region of black box has been expanded as shown on the right. Results revealed interstitial fibrosis (blue stain) in the myocardium of SMTC+Ang II compared with Sham, SMTC and Ang II. The images of the heart tissues were taken at 40X.

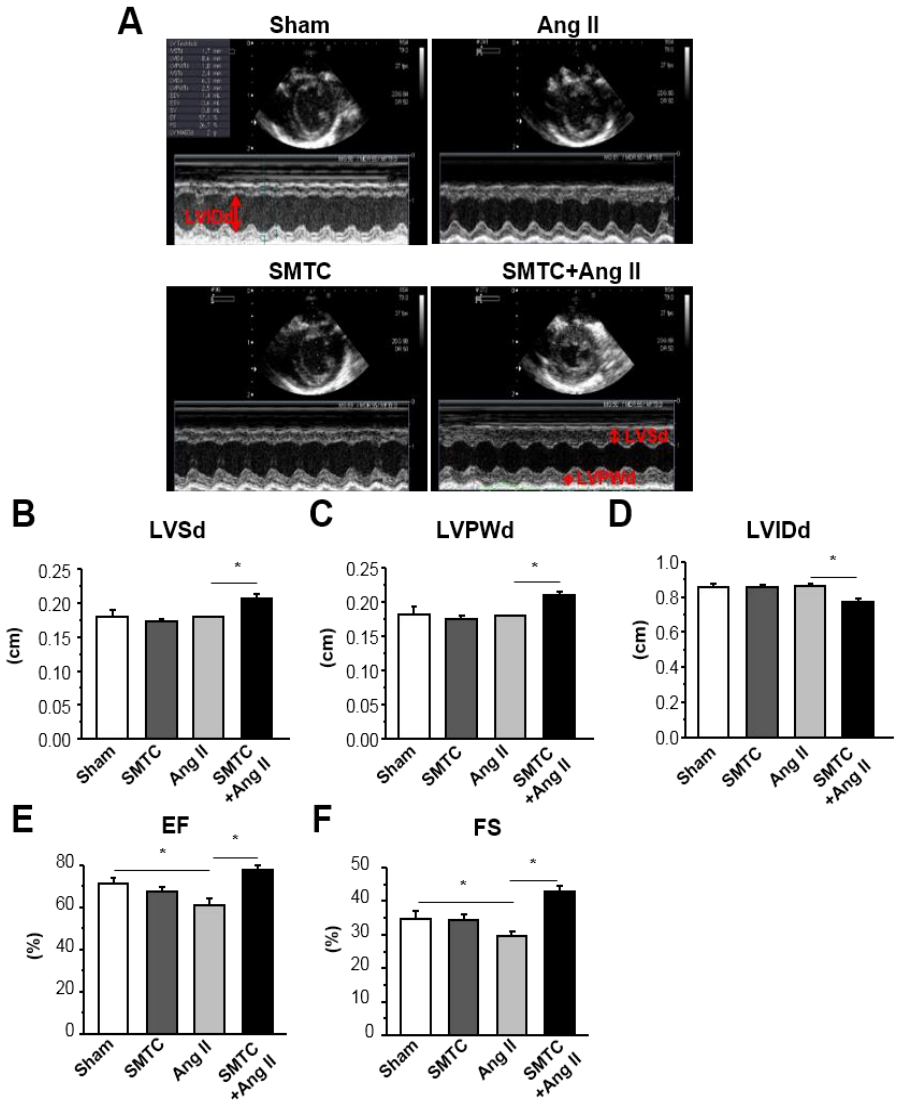
A
Sham
Ang II
SMTC
SMTC+Ang II
LVIDd
LVSd
LVPWd
B
LVSd
C
LVPWd
D
LVIDd
(cm)
E
EF
F
FS
(%)
Sham
SMTC
Ang II
SMTC +Ang II

Figure 19. Echocardiographic assessment of the wall thickness, dimensions and the contractility of LV in Sham, SMTC, Ang II and SMTC+Ang II

(A) Representative echocardiographic images of LV in M-mode. (B) LVSd: the diameter of the left ventricle at diastole was increased in SMTC+Ang II. (C) LVPWd: the diameter of left ventricular posterior wall at diastole was increased in SMTC+Ang II. (D) LVIDd: the inner dimension of left ventricle at diastole was decreased in SMTC+Ang II. (E) EF: Ejection fraction (F) FS: Fractional shortening.

RESULTS

PART 2

Myofilament and sarcomere structure, intracellular Ca^{2+} level and myofilament Ca^{2+} sensitivity in cardiac myocyte following chronic inhibition of nNOS in normal and Ang II–induced hypertensive rats

2–1. nNOS is important in maintaining sarcomere length.

To investigate the effect of nNOS on myocardial structural changes in hypertension, heart tissues of each model were imaged in transmission electron microscopic (TEM) and the morphology of sarcomere were compared before and after nNOS inhibition with and without hypertension. nNOS inhibition in Sham significantly increased the length of sarcomere (μm: 1.87±0.017 in Sham *vs.* 2.12±0.038 in SMTC, $p<0.001$, n=25) and the length of I band (μm: 0.156±0.007 in Sham *vs.* 0.214±0.005 in SMTC, $p<0.001$, n=25) and maintained the length of thick filament (μm: 1.51±0.018 in Sham *vs.* 1.54±0.023 in SMTC, $p=0.3$, n=25, Fig. 20). Whereas nNOS inhibition in hypertension the length of thick filament (μm: 1.49±0.22 in Ang II *vs.* 2.04±0.025 in SMTC+Ang II, $p<0.001$, n=25) and I band (μm: 0.16±0.004 in

Ang II *vs.* 0.28±0.02 in SMTC+Ang II, $p<0.001$, n=25) as well as the sarcomere length (μm: 1.8±0.009 in Ang II *vs.* 2.45±0.06 in SMTC+Ang II, $p<0.001$, n=25) were significantly elongated compared to Ang II (Fig. 20). In addition, detection of α-actinin in immunocytochemistry, a marker of Z-disc, indicated that the peak intensity of α-actinin was significantly increased in SMTC and SMTC+Ang II compared to Sham and Ang II (μm: 1.75±0.01 in Sham *vs.* 1.81±0.028 in SMTC, $p<0.001$, n=146 and 56, 1.72±0.02 in Ang II *vs.* 1.83±0.01 in SMTC+Ang II, $p<0.001$, n=32 and 71, Fig. 21).

In isolated LV myocytes, using a video-sarcomere detection system, the slack length of LV myocyte (without stimulation) was shown to be increased in SMTC ($p<0.001$, between Sham and SMTC, n=68 and 69) and SMTC+Ang II ($p<0.001$, between Ang II and SMTC+Ang II, n=95 and 52, Fig. 22A). Therefore, these results indicate that the activity of nNOS in cardiac myocyte is important in maintaining the sarcomere structure. Conversely, reduced nNOS activity deteriorates cardiac structure and function, adverse remodeling in hypertension.

2-2. nNOS regulates sarcomere shortening, intracellular Ca^{2+} transients and myofilament Ca^{2+} sensitivity in normal and

hypertensive hearts.

The aforementioned results suggest that nNOS has an important role in maintaining the myofilament structure. In order to examine Ca^{2+} transient during cardiac contractility, I measured the sarcomere length and intracellular Ca^{2+} transient under electrical stimulation (2 Hz). Interestingly, unlike the result of slack length without stimulation, sarcomere length of LV myocytes was not increased in Sham, SMTC, Ang II, and SMTC+Ang II under the 2 Hz stimulation condition (p=0.26, between Sham and SMTC, n=19 and 135, p=0.18, between Ang II and SMTC+Ang II, n=27 and 207, Fig. 22B). Because intracellular Ca^{2+} level functions as a central mechanism for sarcomere dynamics, I tested the hypothesis that intracellular Ca^{2+} level could be altered in the models studied. At steady-state contraction, the diastolic Ca^{2+} level was significantly increased in SMTC and SMTC+Ang II compared to Sham and Ang II, respectively (p=0.01, between Sham and SMTC n=28 and 69, p<0.001, between Ang II and SMTC+Ang II, n=32 and 157, Fig. 23B). Peak Ca^{2+} transient was also increased with SMTC in Sham (p=0.05, between Sham and SMTC, n=28 and 69, Fig 23C) and in Ang II (p=0.02 between Ang II and SMTC+Ang

II, n=32 and 157, Fig. 23C). However, delta Ca^{2+} was not changed with SMTC in Sham (p=0.27 between Sham and SMTC, n=28 and 69, Fig. 23D) or with SMTC in Ang II (p=0.89 between SMTC and SMTC+Ang II, n=32 and 157, Fig. 23D). The time constant of Ca^{2+} transient decay (tau, s) was abbreviated in SMTC compared to Sham (p<0.001 between Sham and SMTC, n=31 and n=71) and in SMTC+Ang II compared to Ang II (p<0.001 between SMTC and SMTC+Ang II, n=22 and n=58, Fig. 23E). In line with these results, the time to 50 % relaxation was decreased in SMTC compared to Sham (p<0.001 between Sham and SMTC, n=149 and n=128) or in SMTC+Ang II compared with Ang II (p=0.05 between SMTC and SMTC+Ang II, n=118 and 202, Fig 23F). Sarcomere shortening, in concordance with the delta Ca^{2+} results, was not increased in SMTC and Ang II compared to Sham (p=0.3 between Sham and SMTC, p=0.1 between Sham and Ang II, n=149, 128 and 118 in Sham, SMTC and Ang II, Fig 23G). However, the amplitudes of the sarcomere shortening was significantly increased in SMTC+Ang II compared to Ang II (p=0.04 between Ang II and SMTC+Ang II, n=118 and 202, Fig. 23G).

The lack of change in Ca^{2+} transient with increased sarcomere

shortening indicates that myofilament Ca^{2+} sensitivity could be regulated. Therefore, I analyzed this parameter by recording the sarcomere shortening/relengthening and Ca^{2+} transient simultaneously in Fura-2-loaded LV myocytes and plotted a phase-plane loop of sarcomere length *vs.* Ca^{2+} transient (Fig 24A). As shown in Fig. 24C, relaxation phase of the sarcomere length – Ca^{2+} transient was not changed between Sham and SMTC (50 % sarcomere relengthening: p=0.11, n=28 and 71). However, Myofilament Ca^{2+} sensitivity was reduced in Ang II than in Sham (50 % sarcomere relengthening: p=0.001, between Sham and Ang II, n=28 and 25, Fig 24C). In contrast, sarcomere length – Ca^{2+} transient relationship was shifted to the left in SMTC+Ang II and 50 % sarcomere relengthening was lower than that in Ang II (50 % sarcomere relengthening: p<0.001, between Ang II and SMTC+Ang II, n=25 and 63, Fig 24C).

To identify whether the change in the myofilament Ca^{2+} sensitivity is due to the intrinsic myofilament remodeling rather than the modification with stimulation, I compared the myofilament Ca^{2+} sensitivity of the 1^{st} contraction with stimulation to that of steady-state. At the 1^{st} stimulation, the relaxation phase of the sarcomere length – Ca^{2+} transient

relationship shifted to the left in SMTC and in SMTC+Ang II (Fig. 24B). Accordingly, the values of 50 % sarcomere relengthening of SMTC and SMTC+Ang II were smaller compared to those in Sham and in Ang II, respectively (p<0.001, between Sham and SMTC, n=45 and 52, p<0.001, between Ang II and SMTC+Ang II, n=68 and 42, Fig. 24C), indicative of myofilament Ca^{2+} sensitization. These results suggest that nNOS is essential in maintaining sarcomere structure and regulating myofilament Ca^{2+} sensitivity of LV myocytes from the heart under pressure-overload. In addition, increase of intracellular Ca^{2+} level may be due to the consequence of myofilament remodeling in hypertension.

2-3. Investigation of myofilament protein changes in normal and hypertensive rat models with and without nNOS inhibition

The remodeling of the sarcomere structure and myofilament property in hypertension with nNOS inhibition indicates the possibility of the concomitant changes in the myofilament proteins. Accordingly, immunoblotting was performed in myofilament fraction of LV myocytes to identify the protein abundance of the myofilament proteins. As shown in Fig. 25, the

expressions of the majority of myofilament proteins were not changed in myofilament fraction of LV myocytes lysate from Sham and SMTC (Fig. 25). Distinctively, protein expression of nebulette was significantly increased in SMTC (p=0.01, between Sham and SMTC, n=7, Fig. 25) and in SMTC+Ang II (p=0.05, between Ang II and SMTC+Ang II, n=7, Fig. 26). In addition, the expression of a regulatory troponin protein, troponin I (TnI), was decreased in SMTC+Ang II compared to Ang II (p=0.006, between Ang II and SMTC+Ang II, n=7, Fig. 26).

Taken together, chronic inhibition of nNOS changed the myofilament structure by increasing the sarcomere length, Z-disc morphology, in particular. Accordingly, myofilament Ca^{2+} sensitivity was increased with greater intracellular Ca^{2+} level. These results indicate, *for the first time*, that chronic inhibition of nNOS regulates not only intracellular Ca^{2+} handling but also myofilament structure and function of the heart under pressure-overload.

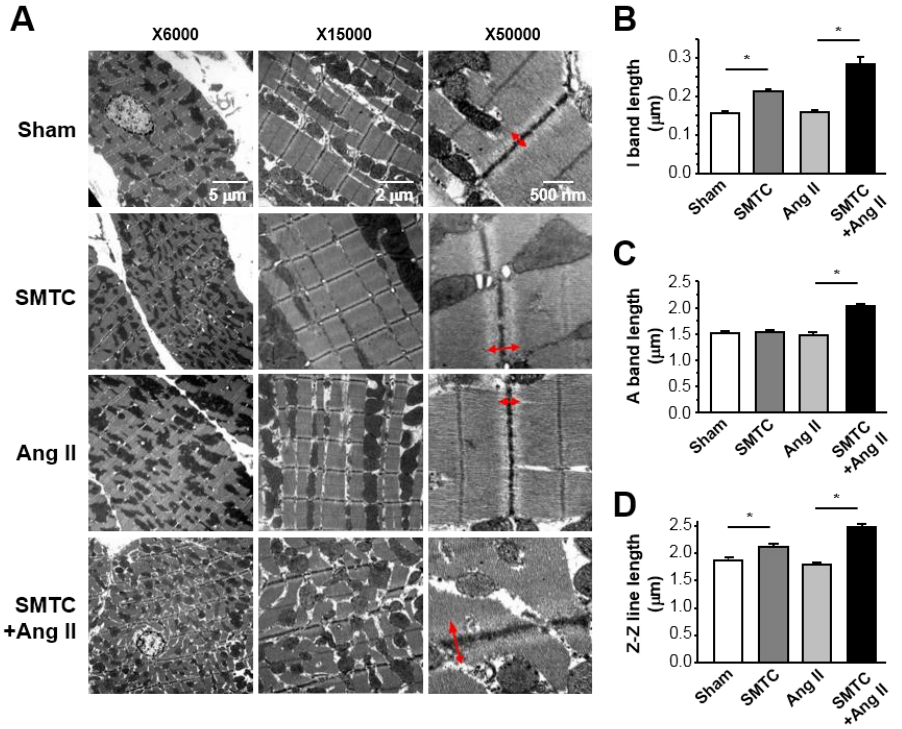

Figure 20. Sarcomere length of LV myocyte in Sham, SMTC, Ang II and SMTC+Ang II

(A) Representative data demonstrating ultrastructural analysis of cardiac sarcomere. Bidirectional arrows (red) indicated I band length. White bars indicated the actual unit value (x6000: 5 μm, x15000: 2 μm, x50000: 500 nm). (B) I band length was calculated at x50000. (C) For measuring the length of the thick filament, A band length was calculated at x15000. (D) Sarcomere length (Z-Z line length) was measured at x15000.

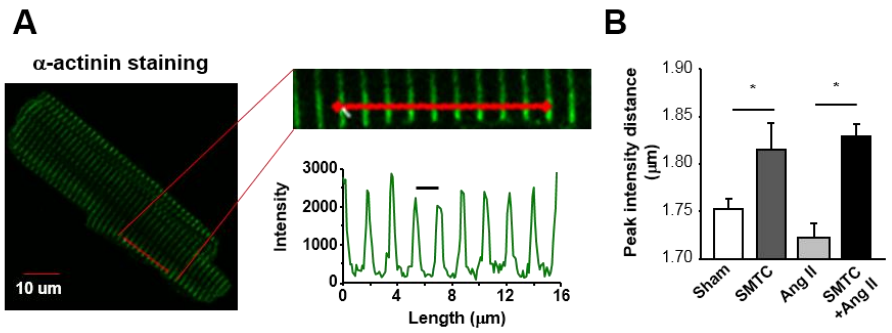

Figure 21. Assessment of the Z-line remodeling (with α-actinin as an indicator) in Sham, SMTC, Ang II and SMTC+Ang II

(A) α-actinin staining (green) indicated the Z-line of LV myocytes. A red line of various lengths was drawn randomly across the LV myocytes. The peak fluorescent intensity (α-actinin) lies on the red line was analyzed as the sarcomere length (bottom right graph). (B) Averaged sarcomere length (distance of α-actinin peak intensity) showed that sarcomere length was increased with nNOS inhibition in Sham and in Ang II.

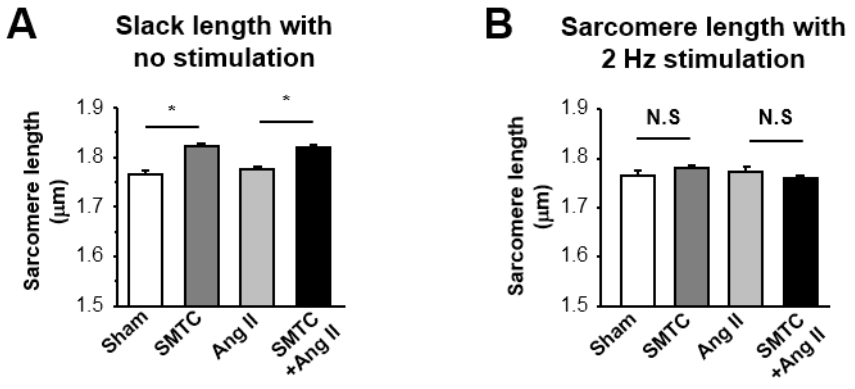

Figure 22. Changes of sarcomere length before and after field stimulation in Sham, SMTC, Ang II and SMTC+Ang II

(A) Slack length of the sarcomere with no stimulation measured by using a video-sarcomere detection system in isolated LV myocytes. (B) Mean value of the diastolic sarcomere length measured with field stimulation at 2 Hz in isolated LV myocytes.

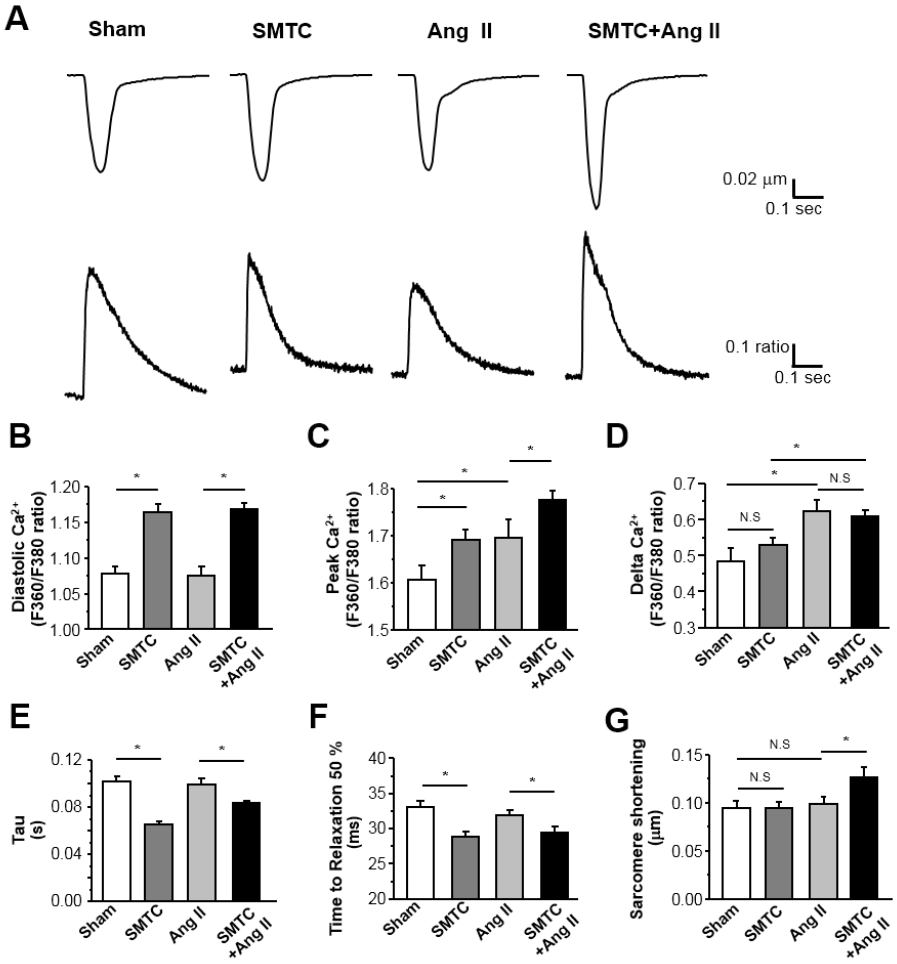
A
Sham
SMTC
Ang II
SMTC+Ang II
0.02 μm
0.1 sec
0.1 ratio
0.1 sec
B
Diastolic Ca2+ (F360/F380 ratio)
1.20
1.15
1.10
1.05
1.00
Sham
SMTC
Ang II
SMTC +Ang II
C
Peak Ca2+ (F360/F380 ratio)
1.8
1.7
1.6
1.5
D
Delta Ca2+ (F360/F380 ratio)
0.7
0.6
0.5
0.4
0.3
N.S
E
Tau (s)
0.12
0.08
0.04
0.00
F
Time to Relaxation 50 % (ms)
40
35
30
25
20
G
Sarcomere shortening (μm)
0.15
0.10
0.05
0.00

Figure 23. Sarcomere shortening and intracellular Ca^{2+} transient with field stimulation in Sham, SMTC, Ang II and SMTC+Ang II

(A) Representative raw traces showed simultaneous recordings of sarcomere shortening/relengthening and intracellular Ca^{2+} transients with field stimulation at 2 Hz in LV myocyte from Sham, SMTC, Ang II and SMTC+Ang II. **(B, C, D)** Mean values of intracellular Ca^{2+} transient, averaged diastolic Ca^{2+} level, averaged peak Ca^{2+} level and averaged delta Ca^{2+} (calculated as the difference between peak Ca^{2+} and diastolic Ca^{2+} ratio). **(E)** Time constant of Ca^{2+} transient decay (tau) was obtained by fitting the decline phase of the Fura-2 ratio with an exponential function. **(F)** Mean values of time to 50 % relaxation. **(G)** Average values of the amplitude of sarcomere shortening (peak height) during contraction.

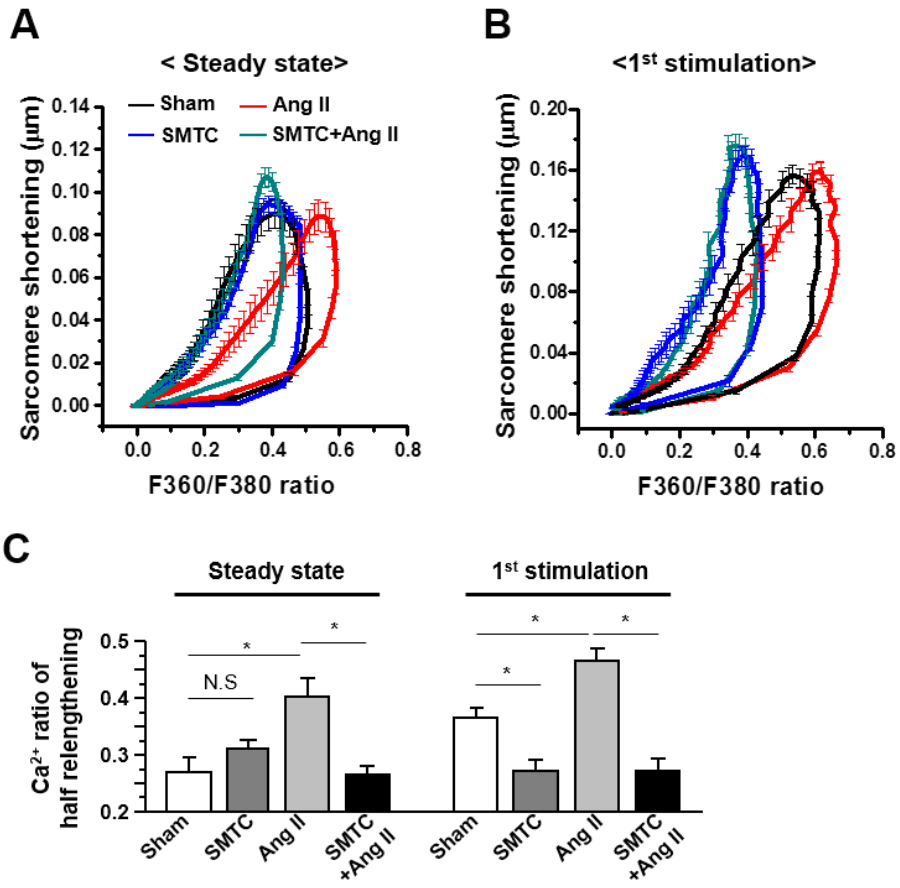

Figure 24. Myofilament Ca^{2+} sensitivity from quiescent to field stimulation in Sham, SMTC, Ang II and SMTC+Ang II

(A) Phase-plane loop of sarcomere shortening/relengthening and intracellular Ca^{2+} transients (delta changes of these parameters) in the steady state after 2 Hz stimulation. (B) Phase-plane loop of sarcomere shortening/relengthening and intracellular Ca^{2+} transient (delta changes of these parameters) at the 1st stimulation (2 Hz). (C) Intracellular Ca^{2+} ratio of half relengthening was obtained as F360/380 ratio of Fura-2 in 50% sarcomere relengthening each of conditions.

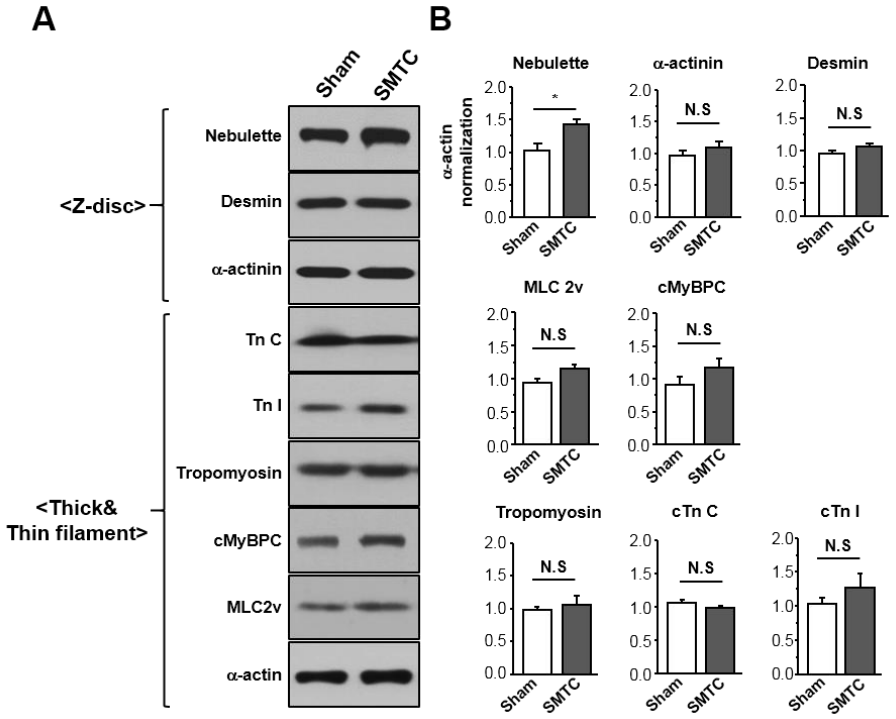

Figure 25. Key proteins in the thick, thin and Z-disc of the myofilament of LV myocytes from Sham and SMTC model

(A) Representative immunoblot images of various myofilament proteins in the myofilament fraction of rat LV myocytes. (B) Averaged mean densities of proteins in LV myocytes from Sham and SMTC. α-actin protein was used as a loading control.

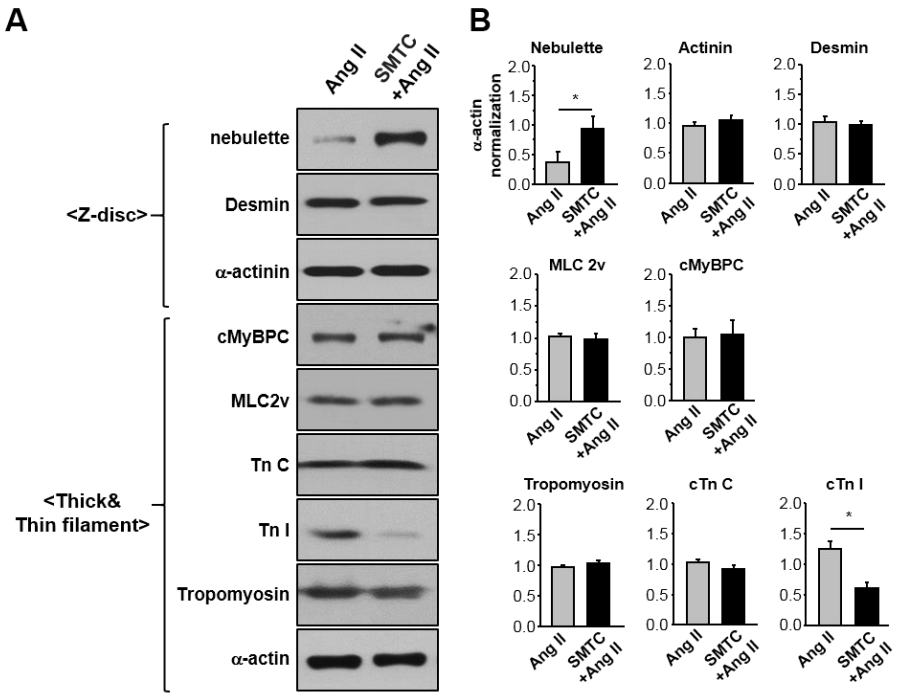

Figure 26. Key proteins in the thick, thin and Z-disc of the myofilament of LV myocytes from Ang II and SMTC+Ang II model

(A) Representative immunoblot images of various myofilament proteins in the myofilament fraction of rat LV myocytes. (B) Averaged mean densities of the proteins in LV myocytes from Ang II and SMTC+Ang II. α-actin protein was used as a loading control.

RESULTS

PART 3

Identification of a novel splice variant of nNOS, nNOSβ, in myofilament fraction of cardiac myocytes from normal and Ang II-induced hypertensive rats with and without nNOS inhibition

I detected genes of alternative splice variants of nNOS in cardiomyocytes using RT-PCR. As shown in Fig. 27, both nNOSα (detected at 534 bp) and nNOSβ (detected at 548 bp) were present in LV myocytes from rat hearts. These results confirm the presence of mRNAs of nNOS splice variants in rat LV myocytes. Protein expressions of nNOS were detected in myofilament and membrane/cytosol fractions of LV myocytes with two different nNOS antibodies (Ab 1 - aa. 1095-1289 and Ab 2 - aa. 2-300, Table 3). nNOS expressions in skeletal muscle and in the brain were also detected for comparison. As shown in Fig. 28A and 28B (left), no nNOS band was detected in membrane/cytosol fractions at short exposure with either antibody. In contrast, there were nNOS bands in myofilament fraction of LV myocytes, skeletal muscle and in the brain, albeit

with different molecular weight: ~140 kDa in the myofilament; both ~140 kDa and 155~165 kDa in skeletal muscle and brain. With longer exposure (Fig. 28A and 28B, right), nNOS proteins became visible in membrane/cytosol fraction of LV myocytes and it appeared as two bands: ~140 kDa and 155~165 kDa. In the myofilament, there was only one band at ~140 kDa. Similar two bands (~140 kDa and 155~165 kDa) in skeletal muscle and one band (155~165 kDa) in the brain were observed with longer exposure. Since nNOSα or μ is known to be at 155~165 kDa and nNOSβ at ~140 kDa, these results indicate that different nNOS splice variants are expressed in different fractions of cardiac myocytes: nNOSα/μ and nNOSβ in the membrane/cytosol and nNOSβ in the myofilament. To determine the presence of nNOS in different fractions of LV myocytes, nNOS was immunoprecipitated in membrane/cytosol and myofilament fractions of LV myocyte lysates and immunoblotted with nNOS antibody (Ab 2). As shown in Fig. 29, nNOS was detected in both membrane/cytosol and in myofilament fractions, with molecular weight ~140 kDa in the myofilament and ~155 kDa in membrane/cytosol. No band was detected with mouse Ig G in both fractions (a negative control). These results further support

that nNOSβ is expressed in myofilament fractions of LV myocytes from rat heart.

Next, I observed whether nNOSβ in myofilament fraction was altered in Sham and SMTC. Unexpectedly, nNOSβ protein expression was increased in the myofilament fraction of SMTC rat hearts (p<0.001 between Sham and SMTC, n=8, Fig. 30), but nNOSα/μ was not increased, which is different compared to Sham in membrane/cytosol fraction (p=0.75 between Sham and SMTC, n=8, Fig. 30). Also, nNOSβ protein expression was increased in the myofilament fraction of SMTC+Ang II rat hearts (p<0.001 between Ang II and SMTC+Ang II, n=8, Fig. 31).

These results showed that nNOSβ was expressed in the myofilament of cardiac myocytes; the protein expression of which was increased with chronic inhibition of nNOS in healthy heart and that in hypertension.

Table 3. Antibodies of nNOS used in the current study

	Antibody (Supplier)	Antigen (nNOS peptide)	Detection (nNOS splicing variants)
Ab-1	BD Bioscience (610309)	aa 1095-1289	α, β, μ, γ, nNOS-2 form
Ab-2	A-11, SANTA CRUZ (SC-5302)	aa 2-300	α, β, μ, γ, nNOS-2 form

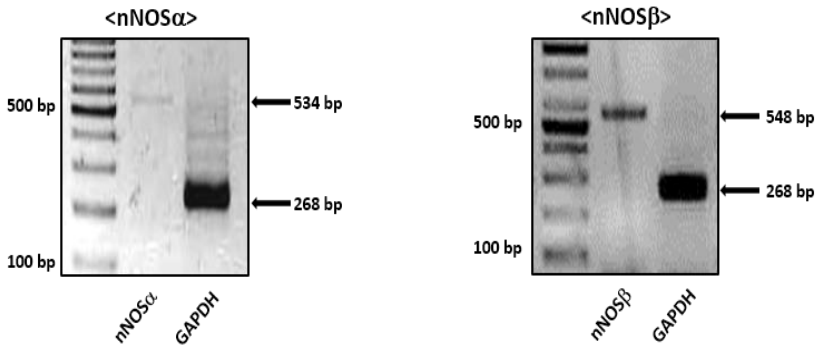

Figure 27. Expressions of nNOSα and nNOSβ mRNA in rat LV myocytes

nNOSα was detected using a forward primer targeting exon 1a and a reverse primer targeting exon 2. nNOSβ was detected using a forward primer targeting exon 1a and a reverse primer targeting exon 6. GAPDH was used as an internal control. DNA ladder was shown on the left.

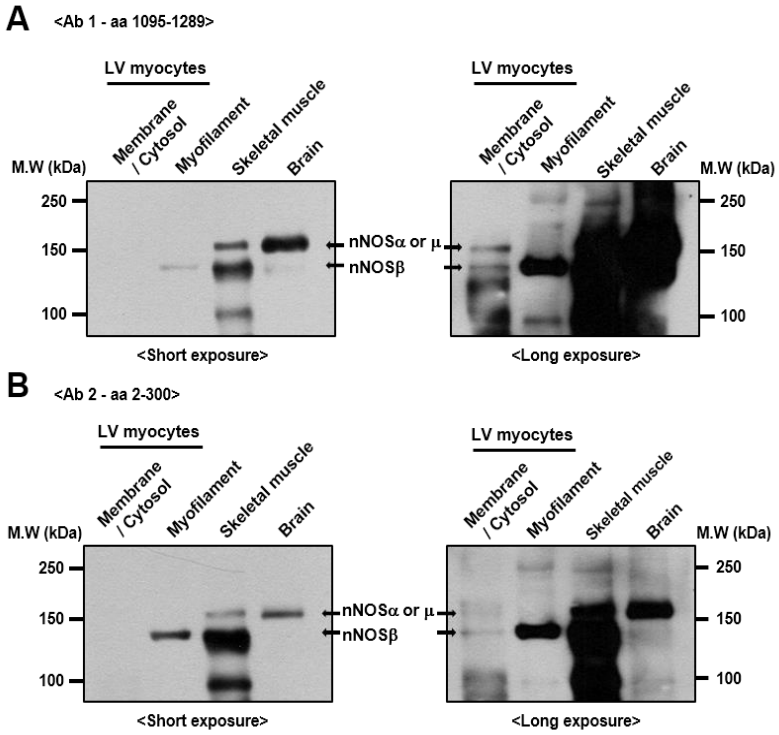

Figure 28. Detection of nNOS protein expression in membrane/cytosol and myofilament fractions of rat LV myocytes using two different antibodies

Immunoblotting was conducted in subfraction of LV myocytes with nNOS antibodies. **(A)** A1−aa. 1095~1289 and **(B)** A2−aa. 2~300. Short exposure (~30 s) revealed ~140 kDa protein in myofilament, indicate nNOSβ. Long exposure (>1 min) revealed proteins at 155 kDa and at ~140 kDa, in membrane/cytosol fraction and one ~140 kDa band in myofilament indicating nNOSα/μ (160~165 kDa) and nNOSβ (~140 kDa), respectively. Skeletal muscle and brain tissue were used as positive controls.

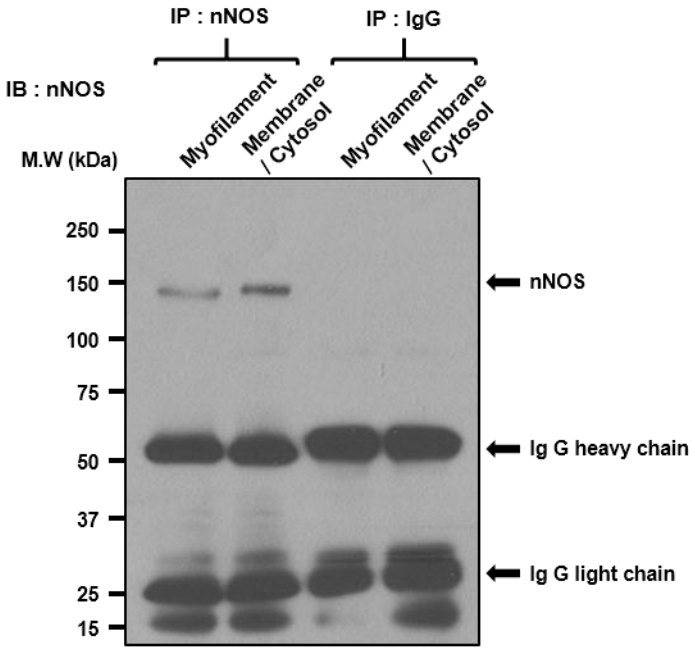

Figure 29. Immunoprecipitation of nNOS protein in membrane/ cytosol and myofilament fractions of rat LV myocytes

Immunoprecipitation was conducted in respective subfraction of LV myocytes. Mouse IgG was used as a negative control. Results showed that nNOS (~140 kDa) was detected in myofilament fraction, indicating nNOSβ. In membrane/cytosol fraction, immunoprecipitated nNOS protein was around ~155 kDa. No band was observed with IgG. n=5.

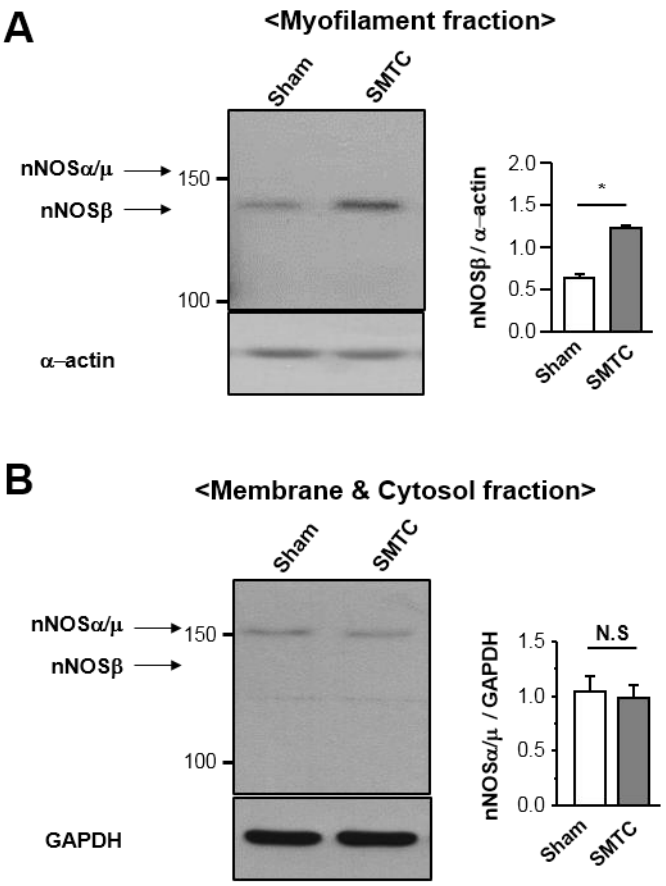

Figure 30. nNOS protein expression in the membrane/cytosol and myofilament fractions of LV myocytes from Sham and SMTC

(A) In myofilament fraction, nNOSβ (~140 kDa) was increased in SMTC. (B) In membrane & cytosol fraction, nNOSα/μ (155 kDa) was detected and not changed between Sham and SMTC. For the quantitive comparison, α−actin and GAPDH were used as a loading control in each of subfraction.

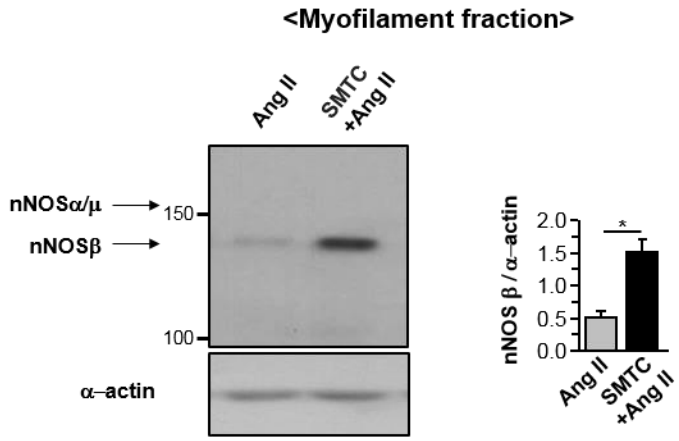

Figure 31. nNOS protein expression in the myofilament fractions of LV myocytes from Ang II and SMTC+Ang II

In myofilament fraction, nNOSβ (~140 kDa) was increased in SMTC+Ang II. For the quantitive comparison, α-actin was used as a loading control in each of subfraction.

RESULTS

PART 4

Myofilament and sarcomere structure in cardiac myocyte from nNOSα/μ null mice

nNOSβ protein is expressed in the myofilament fraction of LV myocyte from nNOSα/μ null mice.

Immunoblotting of the expressions of nNOS in the membrane/cytosol and myofilament fractions was performed in LV myocytes from $nNOS^{+/+}$ and $nNOS\alpha/\mu^{-/-}$ mice to confirm the expressions of nNOS in the myofilament. As shown in Fig. 32, nNOS proteins were detected in membrane/cytosol and myofilament fractions of LV myocytes, skeletal muscle and the brain from $nNOS^{+/+}$ and $nNOS^{-/-}$ mice (both 155~165 kDa and ~140 kDa bands in membrane/cytosol fractions of LV myocytes and skeletal muscle; ~140 kDa band in the myofilament and 155~165 kDa band in the brain). Therefore, nNOSβ protein was expressed in both membrane/cytosol fraction of skeletal muscle and the myofilament fractions of LV of $nNOS\alpha/\mu^{-/-}$, but the expression level was lower than that from wild type mice (Fig. 32). Next, I identified the myofilament ultrastructure of the LV

of nNOSα/μ$^{-/-}$ and nNOSα/μ$^{+/+}$ mice using TEM analysis. Unlike pharmacological inhibition of nNOS in rats, there was no difference in sarcomere structure of LV myocytes between the two groups (nNOS$^{+/+}$ μm: 1.67±0.03; nNOSα/μ$^{-/-}$, μm: 1.66±0.02) (Fig. 33D). In addition, the lengths of I band, A band or sarcomere length were not different between the groups (μm: 0.31±0.01 in nNOS$^{+/+}$ *vs.* 0.32±0.02 in nNOSα/μ$^{-/-}$, Fig. 33B; μm: 1.24±0.02 in nNOS$^{+/+}$ *vs.* 1.27±0.01 in nNOSα/μ$^{-/-}$, Fig. 33C).

Furthermore, immunoblotting results showed that the expressions of various myofilament proteins of the Z-disc, thick and thin filament in the myofilament fraction of the heart were not different between nNOS$^{+/+}$ and nNOSα/μ$^{-/-}$ mice (Fig. 34). These results suggest that, nNOSα/μ gene deletion in mice does not affect myofilament morphology and sarcomere length of the heart in the absence of pathological stimuli, such as pressure-overload.

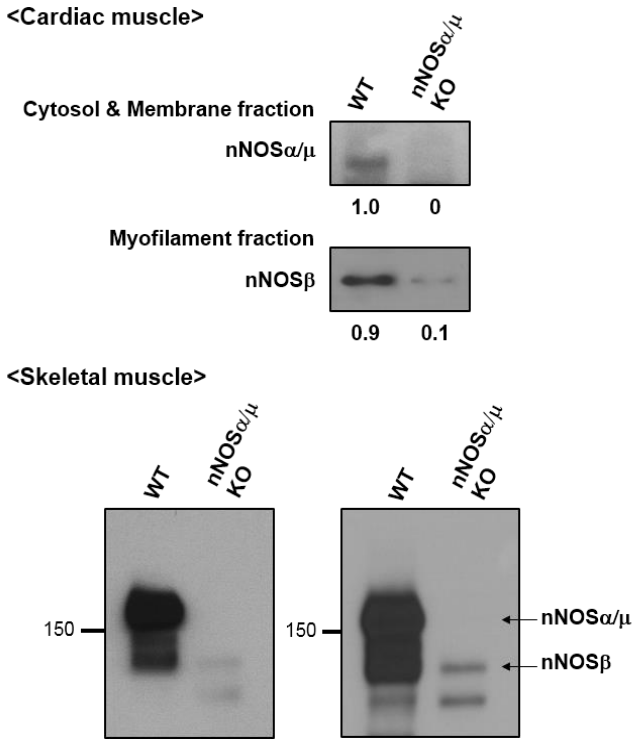

Figure 32. Identification of nNOS splice variants in membrane/ cytosol and myofilament fractions of LV tissue in $nNOS^{+/+}$ and $nNOS^{-/-}$ mice

Upper panel: protein expressions of nNOSα/μ and nNOSβ in the cytosol & membrane and myofilament fractions of cardiac muscle.

Lower panel: in skeletal muscle, both nNOSα/μ and nNOSβ protein were detected in cytosol & membrane fraction of LV myocytes.

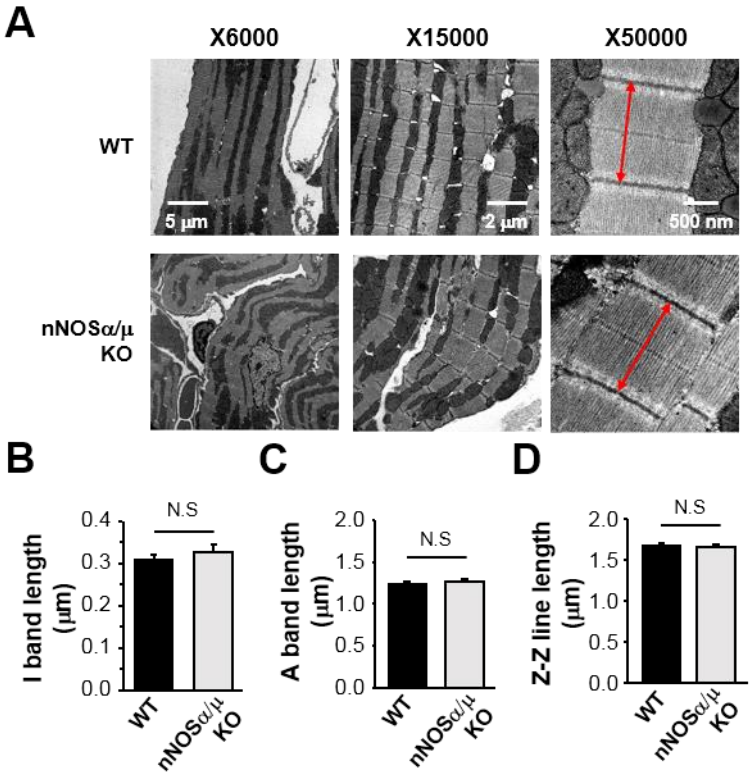

Figure 33. Sarcomere length of LV in WT and NOSα/μ null mice

(A) Representative data demonstrating ultrastructure of LV myocardium. Bidirectional arrows (red) indicated the sarcomere length. White bars indicated the actual unit value (x6000: 5 μm, x15000: 2 μm, x50000: 500 nm). (B–D) I band length was calculated at x50000. Thick filament length (A band) length was calculated at x15000. Sarcomere (Z–Z line) length was calculated at x15000.

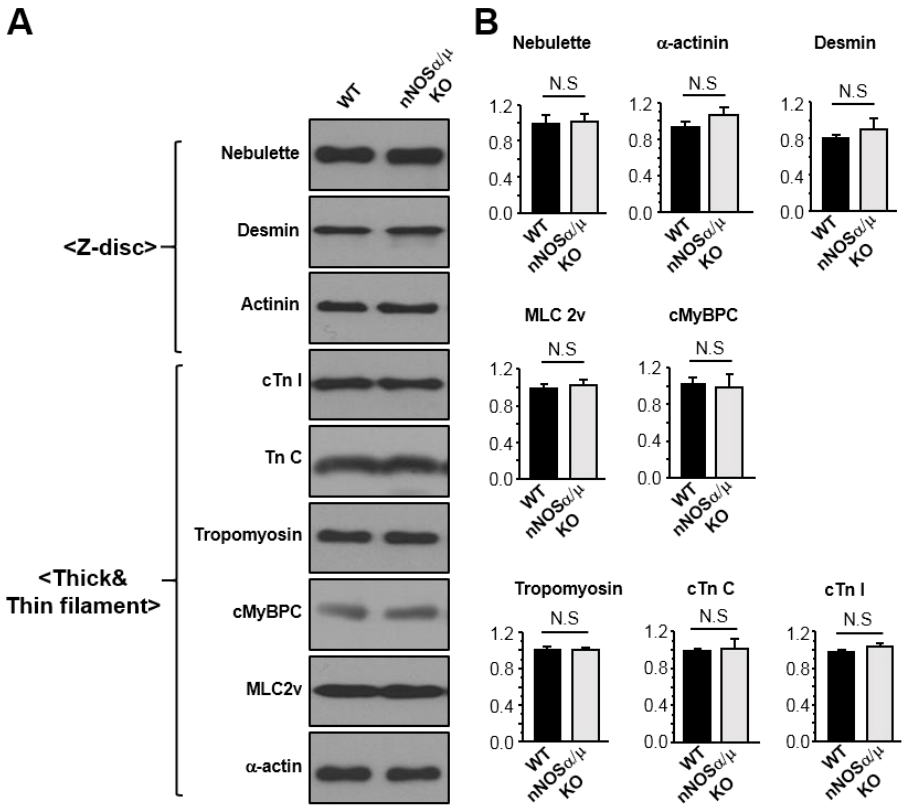

Figure 34. The key proteins in the thick, thin and Z-disc of the sarcomere in LV tissue from WT and nNOSα/μ null mice

(A) Representative immunoblot images of myofilament proteins in the myofilament fraction of LV from WT and nNOSα/μ null mice. (B) Averaged ratio of myofilament proteins of LV in WT and nNOSα/μ null mice. α-actin protein was used as the loading control.

DISCUSSION

In the present study, I demonstrated direct evidence to show that nNOS protein was expressed in the myofilament fraction of LV myocytes from rat heart and nNOS is critical in protecting the heart from disease progression under pressure-overload. Evidence supporting the findings are: **Part 1)** Inhibition of all active nNOS (nNOSα/μ/β) using SMTC in Ang II-infusing hypertensive rats induced concentric hypertrophy in LV myocardium, as indicated by morphological and functional changes of the heart; **Part 2)** Chronic inhibition of nNOSα/μ/β increased sarcomere length of the myocardium, increased myofilament Ca^{2+} sensitivity and intracellular Ca^{2+} level during contraction; **Part 3)** A distinctive nNOS splice variant (nNOSβ, 140 kDa) is expressed in the myofilament of LV myocytes. The expression of which was not different between Sham and Ang II but it is significantly increased in SMTC and SMTC+Ang II; **Part 4)** nNOSβ is expressed in the myofilament fraction in nNOSα/μ null mice. Deletion of nNOSα/μ did not affect sarcomere length, indicating the functional relevance of nNOSβ in structural

remodeling of myocardium under normal and pressure-overload conditions (Fig. 35).

Putative roles of nNOSβ in the cardiac myocytes.

Our results implied that NOSβ is expressed in the myofilament to have a function of maintaining the myofilament structure. Previously, we have shown that acute inhibition of nNOS with a specific inhibitor (SMTC, inhibit all three splice variants of nNOS, nNOSα/μ/β) was associated with increased myofilament Ca^{2+} sensitivity in LV myocytes from hypertensive rats, mediated by the phosphorylations of TnI and cMyBPC *via* nNOS/cGMP/PKG-dependent pathway (Jin, Jang et al. 2013). These results suggest a new role of nNOS in the regulation of myofilament property. However, it was questionable whether nNOS could exert these functions in the myofilament, *in situ*. Since nNOSα/μ are the only splice variants of nNOS those are detected in the cytosol/membrane fraction of cardiac myocytes and are studied intensively in cardiac physiology and pathology, our results with the identification of nNOS in the myofilament is essential in understanding the mechanism of nNOS in the myofilament regulation.

The role of nNOSβ in the myofilament is unclear. My results show that inhibition of nNOS (nNOSα/μ/β) significantly increased nebulette protein (cardiac specific isoform in the nebulin repeat protein) in myofilament fraction of LV myocytes (Fig. 24). Whereas proteins in the majority of thin, thick filament and Z-disc representing in the lateral boundary of the sarcomere (Frank and Frey 2011), was unaffected. Since nebulin family proteins, such as nebulin and lasp, are known to play an important role in Z-Z length regulation and force transduction (Witt, Burkart et al. 2006, Fernandes and Schock 2014), the increase of nebulette in myofilament might contribute to the increase of sarcomere length in LV myocytes from SMTC. It is suggested that activation of nNOSβ probably contributes to anchoring the nebulette in the Z-disc.

Interestingly, the increase of the sarcomere length was disappeared under the condition of excitation, which was the reason of compensated for the increase of diastolic Ca^{2+} in myocytes. In addition, myofilament Ca^{2+} sensitivity was increased in SMTC compared with Sham with the 1^{st} electrical stimulation. However, more research is needed as to whether

nNOSβ in the myofilament has the direct role in relation to intracellular Ca^{2+} regulation.

Taken together, Ang II-induced hypertension prompted severe pressure overload to the heart, especially with nNOS inhibition. Consequently, myocardial hypertrophy is developed, which was confirmed by the current study. Therefore, nNOSβ may protect the myocardium from the pathological overload by maintaining the cardiac structure and function.

nNOSβ in the other tissue

It is well acknowledged that nNOS splice variants are distributed in different compartments within the same types of cells. E.g., nNOSμ has been shown to be distributed in sarcolemma in skeletal muscle (Brenman, Chao et al. 1995, Chao, Gorospe et al. 1996, Kameya, Miyagoe et al. 1999, Crosbie, Barresi et al. 2002). Recent report by Percival et al. also showed that nNOSβ splice variant is located in Golgi compartment and plays an important part in maintaining the skeletal muscle contractility during and after exercise (Percival, Anderson et al. 2010). Similarly, previous report in centrifugation-dependent subcellular fraction has shown that both nNOSα and nNOSβ may

be expressed in sarcolemma enriched fraction of skeletal muscle (Baum, Schlappi et al. 2011), although the presence of nNOSα in skeletal muscle is questioned. nNOSβ-dependent NO in Golgi is suggested to regulate muscle contractility *via* posttranslational modifications (e.g. cGMP-dependent phosphorylation) due to co-localization of soluble guanylate cyclase and PKG (Percival, Anderson et al. 2010). By the same token, nNOSβ is known to contribute to a major portion of NO-dependent penile erection, even in the absence of nNOSα (Hurt, Sezen et al. 2006). In kidney, where both nNOSα and β proteins are expressed (Smith, Merchant et al. 2009), NO generation from nNOSβ in macula densa cells is functionally important in tubule glomerular feedback during salt loading (Lu, Fu et al. 2010). These reports demonstrate the expression and the important roles of nNOSβ in various tissues.

nNOSβ in nNOSα/μ knockout mice

Our results using nNOSα/$\mu^{-/-}$ mice showed that the protein expression of nNOSβ is maintained in the myofilament, although nNOSα/μ gene deleted in the cytosol & membrane fraction. These results are consistent with the notion that nNOSα/$\mu^{-/-}$ mice were

generated by replacing exon 2 to target nNOSα/μ (by deletion of PDZ binding motif)(Huang, Dawson et al. 1993), thus nNOSβ should be maintained in theory. In fact, studies using nNOSα/μ$^{-/-}$ mice have shown certain degree of nNOS activity, suggesting that the residual nNOS splice variants are active, possibly through nNOSβ (Putzke, Seidel et al. 2000, Hurt, Sezen et al. 2006). nNOSβ was expressed in the myocardium of nNOSα/μ$^{-/-}$ mice, which is in accordance with other groups, although the quantification of protein was lower than those in wild type. It is not known whether the nNOSα/μ gene may affect nNOSβ translation in cardiac myocyte. So far, no nNOSβ-specific knockout mice are available yet, which is the main limitation of the current study.

There is another line of nNOS null mice, KN2 (exon 6 replaced to target all nNOS splice variants by disrupting heme-binding domain) (Gyurko, Leupen et al. 2002). The expression of nNOS splice variants in the myofilament fraction of these mice hearts have not been studied yet.

In summary, these results show that nNOS splice variants at discrete localizations play in concert to coordinate for the

desirable functions in the cardiac mechanics. Especially, nNOSβ in the myofilament fraction may directly affect cardiac structure and function by targeting the proteins in the myofilament, intracellular Ca^{2+} handling as well as signaling pathways in healthy heart and those under pathological stress.

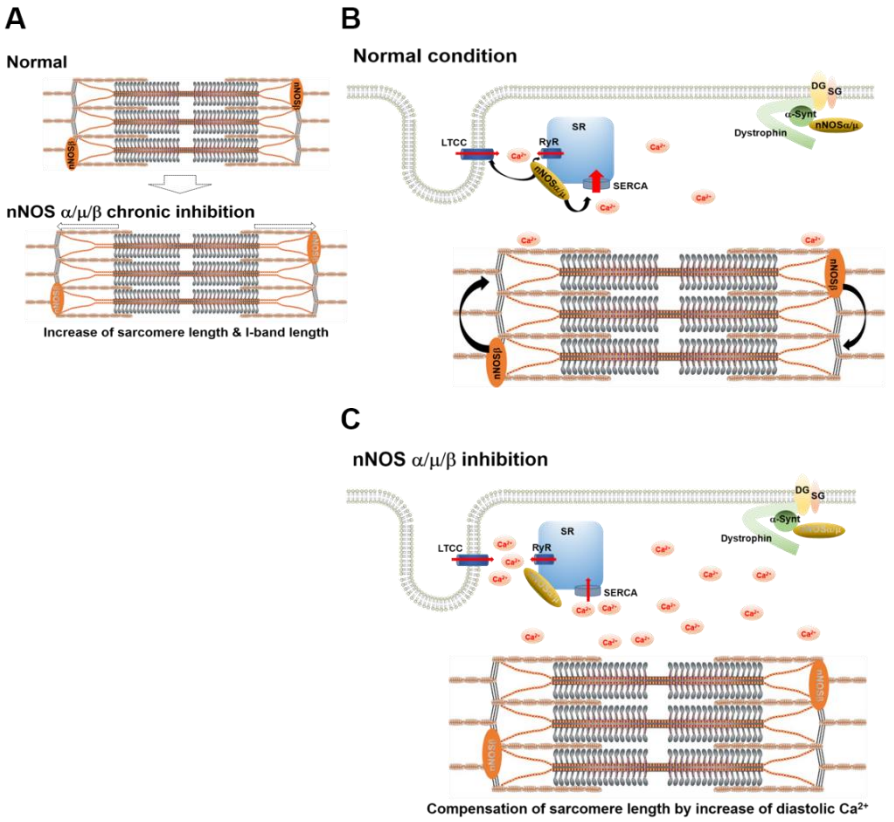

Figure 35. Schematic diagram of hypothesized mechanisms for the roles of nNOS splice variants in cardiac myocyte.

(A) Inhibition of nNOS with SMTC significantly increased the sarcomere and I band lengths of the LV myocyte from Sham and Ang II–induced hypertensive rats. (B, C) With field stimulation of LV myocytes at 2 Hz, both diastolic and systolic Ca^{2+} were increased and sarcomere length was maintained with nNOS inhibition compared to Sham. Furthermore, nNOSβ is responsible for the regulation of myofilament Ca^{2+} sensitivity in the hearts from hypertensive rats.

REFERENCES

Adachi, T., R. M. Weisbrod, D. R. Pimentel, J. Ying, V. S. Sharov, C. Schoneich and R. A. Cohen (2004). "S-Glutathiolation by peroxynitrite activates SERCA during arterial relaxation by nitric oxide." Nat Med 10(11): 1200-1207.

Alderton, W. K., C. E. Cooper and R. G. Knowles (2001). "Nitric oxide synthases: structure, function and inhibition." Biochem J 357(Pt 3): 593-615.

Aragon, J. P., M. E. Condit, S. Bhushan, B. L. Predmore, S. S. Patel, D. B. Grinsfelder, S. Gundewar, S. Jha, J. W. Calvert, L. A. Barouch, M. Lavu, H. M. Wright and D. J. Lefer (2011). "Beta3-adrenoreceptor stimulation ameliorates myocardial ischemia-reperfusion injury via endothelial nitric oxide synthase and neuronal nitric oxide synthase activation." J Am Coll Cardiol 58(25): 2683-2691.

Barouch, L. A., T. P. Cappola, R. W. Harrison, J. K. Crone, E. R. Rodriguez, A. L. Burnett and J. M. Hare (2003). "Combined loss of neuronal and endothelial nitric oxide synthase causes premature mortality and age-related hypertrophic cardiac remodeling in mice." J Mol Cell Cardiol 35(6): 637-644.

Barouch, L. A., R. W. Harrison, M. W. Skaf, G. O. Rosas, T. P. Cappola, Z. A. Kobeissi, I. A. Hobai, C. A. Lemmon, A. L. Burnett, B. O'Rourke, E. R. Rodriguez, P. L. Huang, J. A. Lima, D. E. Berkowitz and J. M. Hare (2002). "Nitric oxide regulates the heart by spatial confinement of nitric oxide synthase isoforms." Nature 416(6878): 337-339.

Baum, O., S. Schlappi, F. A. Huber-Abel, A. Weichert, H. Hoppeler and A. Zakrzewicz (2011). "The beta-isoform of neuronal nitric oxide synthase (nNOS) lacking the PDZ domain is localized at the sarcolemma." FEBS Lett 585(20): 3219-3223.

Bendall, J. K., T. Damy, P. Ratajczak, X. Loyer, V. Monceau, I. Marty, P. Milliez, E. Robidel, F. Marotte, J. L. Samuel and C. Heymes (2004). "Role of myocardial neuronal nitric oxide synthase-derived nitric oxide in beta-adrenergic hyporesponsiveness after myocardial infarction-induced heart failure in rat." Circulation 110(16): 2368-2375.

Bernardo, B. C., K. L. Weeks, L. Pretorius and J. R. McMullen (2010). "Molecular distinction between physiological and pathological cardiac hypertrophy: experimental findings and therapeutic strategies." Pharmacol Ther 128(1): 191-227.

Bohlen, H. G. (2015). "Nitric oxide and the cardiovascular system." Compr Physiol 5(2): 808-823.

Brede, M., W. Roell, O. Ritter, F. Wiesmann, R. Jahns, A. Haase, B. K. Fleischmann and L. Hein (2003). "Cardiac hypertrophy is associated with decreased eNOS expression in angiotensin AT2 receptor-deficient mice." Hypertension 42(6): 1177-1182.

Brenman, J. E., D. S. Chao, S. H. Gee, A. W. McGee, S. E. Craven, D. R. Santillano, Z. Wu, F. Huang, H. Xia, M. F. Peters, S. C. Froehner and D. S. Bredt (1996). "Interaction of nitric oxide synthase with the postsynaptic density protein PSD-95 and alpha1-syntrophin mediated by PDZ domains." Cell 84(5): 757-767.

Brenman, J. E., D. S. Chao, H. Xia, K. Aldape and D. S. Bredt (1995).

"Nitric oxide synthase complexed with dystrophin and absent from skeletal muscle sarcolemma in Duchenne muscular dystrophy." Cell 82(5): 743-752.

Burger, D. E., X. Lu, M. Lei, F. L. Xiang, L. Hammoud, M. Jiang, H. Wang, D. L. Jones, S. M. Sims and Q. Feng (2009). "Neuronal nitric oxide synthase protects against myocardial infarction-induced ventricular arrhythmia and mortality in mice." Circulation 120(14): 1345-1354.

Burkard, N., T. Williams, M. Czolbe, N. Blomer, F. Panther, M. Link, D. Fraccarollo, J. D. Widder, K. Hu, H. Han, U. Hofmann, S. Frantz, P. Nordbeck, J. Bulla, K. Schuh and O. Ritter (2010). "Conditional overexpression of neuronal nitric oxide synthase is cardioprotective in ischemia/reperfusion." Circulation 122(16): 1588-1603.

Cai, H., Z. Li, S. Dikalov, S. M. Holland, J. Hwang, H. Jo, S. C. Dudley, Jr. and D. G. Harrison (2002). "NAD(P)H oxidase-derived hydrogen peroxide mediates endothelial nitric oxide production in response to angiotensin II." J Biol Chem 277(50): 48311-48317.

Chao, D. S., J. R. Gorospe, J. E. Brenman, J. A. Rafael, M. F. Peters, S. C. Froehner, E. P. Hoffman, J. S. Chamberlain and D. S. Bredt (1996). "Selective loss of sarcolemmal nitric oxide synthase in Becker muscular dystrophy." J Exp Med 184(2): 609-618.

Chow, B. S., M. Kocan, S. Bosnyak, M. Sarwar, B. Wigg, E. S. Jones, R. E. Widdop, R. J. Summers, R. A. Bathgate, T. D. Hewitson and C. S. Samuel (2014). "Relaxin requires the angiotensin II type 2 receptor to abrogate renal interstitial fibrosis." Kidney Int 86(1): 75-85.

Copp, S. W., D. M. Hirai, S. K. Ferguson, C. T. Holdsworth, T. I. Musch and D. C. Poole (2012). "Effects of chronic heart failure on neuronal nitric oxide synthase-mediated control of microvascular O2 pressure in contracting rat skeletal muscle." J Physiol 590(15): 3585-3596.

Crosbie, R. H., R. Barresi and K. P. Campbell (2002). "Loss of sarcolemma nNOS in sarcoglycan-deficient muscle." FASEB J 16(13): 1786-1791.

Cunningham, M. W., Jr., J. M. Sasser, C. A. West and C. Baylis (2013). "Renal redox response to normal pregnancy in the rat." Am J Physiol Regul Integr Comp Physiol 304(6): R443-449.

Damy, T., P. Ratajczak, E. Robidel, J. K. Bendall, P. Oliviero, J. Boczkowski, T. Ebrahimian, F. Marotte, J. L. Samuel and C. Heymes (2003). "Up-regulation of cardiac nitric oxide synthase 1-derived nitric oxide after myocardial infarction in senescent rats." FASEB J 17(13): 1934-1936.

Damy, T., P. Ratajczak, A. M. Shah, E. Camors, I. Marty, G. Hasenfuss, F. Marotte, J. L. Samuel and C. Heymes (2004). "Increased neuronal nitric oxide synthase-derived NO production in the failing human heart." Lancet 363(9418): 1365-1367.

Dawson, D., C. A. Lygate, M. H. Zhang, K. Hulbert, S. Neubauer and B. Casadei (2005). "nNOS gene deletion exacerbates pathological left ventricular remodeling and functional deterioration after myocardial infarction." Circulation 112(24): 3729-3737.

Eliasson, M. J., S. Blackshaw, M. J. Schell and S. H. Snyder (1997). "Neuronal nitric oxide synthase alternatively spliced forms: prominent functional localizations in the brain." Proc Natl Acad Sci

U S A 94(7): 3396-3401.

Fernandes, I. and F. Schock (2014). "The nebulin repeat protein Lasp regulates I-band architecture and filament spacing in myofibrils." J Cell Biol 206(4): 559-572.

Feron, O., L. Belhassen, L. Kobzik, T. W. Smith, R. A. Kelly and T. Michel (1996). "Endothelial nitric oxide synthase targeting to caveolae. Specific interactions with caveolin isoforms in cardiac myocytes and endothelial cells." J Biol Chem 271(37): 22810-22814.

Flaherty, M. P., M. Brown, I. L. Grupp, J. E. Schultz, S. S. Murphree and W. K. Jones (2007). "eNOS deficient mice develop progressive cardiac hypertrophy with altered cytokine and calcium handling protein expression." Cardiovasc Toxicol 7(3): 165-177.

Flogel, U., M. W. Merx, A. Godecke, U. K. Decking and J. Schrader (2001). "Myoglobin: A scavenger of bioactive NO." Proc Natl Acad Sci U S A 98(2): 735-740.

Frank, D. and N. Frey (2011). "Cardiac Z-disc signaling network." J Biol Chem 286(12): 9897-9904.

Gao, J., H. Zhang, K. D. Le, J. Chao and L. Gao (2011). "Activation of central angiotensin type 2 receptors suppresses norepinephrine excretion and blood pressure in conscious rats." Am J Hypertens 24(6): 724-730.

Gao, J., I. H. Zucker and L. Gao (2014). "Activation of central angiotensin type 2 receptors by compound 21 improves arterial baroreflex sensitivity in rats with heart failure." Am J Hypertens 27(10): 1248-1256.

Gonzalez, D. R., F. Beigi, A. V. Treuer and J. M. Hare (2007). "Deficient ryanodine receptor S-nitrosylation increases sarcoplasmic reticulum calcium leak and arrhythmogenesis in cardiomyocytes." Proc Natl Acad Sci U S A 104(51): 20612-20617.

Grossman, W., D. Jones and L. P. McLaurin (1975). "Wall stress and patterns of hypertrophy in the human left ventricle." J Clin Invest 56(1): 56-64.

Gyurko, R., S. Leupen and P. L. Huang (2002). "Deletion of exon 6 of the neuronal nitric oxide synthase gene in mice results in hypogonadism and infertility." Endocrinology 143(7): 2767-2774.

Heusch, G., H. Post, M. C. Michel, M. Kelm and R. Schulz (2000). "Endogenous nitric oxide and myocardial adaptation to ischemia." Circ Res 87(2): 146-152.

Heusch, G. and R. Schulz (2011). "A radical view on the contractile machinery in human heart failure." J Am Coll Cardiol 57(3): 310-312.

Huang, A., D. Sun, E. G. Shesely, E. M. Levee, A. Koller and G. Kaley (2002). "Neuronal NOS-dependent dilation to flow in coronary arteries of male eNOS-KO mice." Am J Physiol Heart Circ Physiol 282(2): H429-436.

Huang, P. L., T. M. Dawson, D. S. Bredt, S. H. Snyder and M. C. Fishman (1993). "Targeted disruption of the neuronal nitric oxide synthase gene." Cell 75(7): 1273-1286.

Huisamen, B., S. J. Perel, S. O. Friedrich, R. Salie, H. Strijdom and A. Lochner (2011). "ANG II type I receptor antagonism improved

nitric oxide production and enhanced eNOS and PKB/Akt expression in hearts from a rat model of insulin resistance." Mol Cell Biochem 349(1-2): 21-31.

Hurt, K. J., S. F. Sezen, H. C. Champion, J. K. Crone, M. A. Palese, P. L. Huang, A. Sawa, X. Luo, B. Musicki, S. H. Snyder and A. L. Burnett (2006). "Alternatively spliced neuronal nitric oxide synthase mediates penile erection." Proc Natl Acad Sci U S A 103(9): 3440-3443.

Ignarro, L. J., R. G. Harbison, K. S. Wood and P. J. Kadowitz (1986). "Activation of purified soluble guanylate cyclase by endothelium-derived relaxing factor from intrapulmonary artery and vein: stimulation by acetylcholine, bradykinin and arachidonic acid." J Pharmacol Exp Ther 237(3): 893-900.

Ihara, H., M. Kuwamura, M. Atsuta, I. Nihonmatsu, T. Okada, M. Mukamoto and S. Kozaki (2006). "Expression of neuronal nitric oxide synthase variant, nNOS-mu, in rat brain." Nitric Oxide 15(1): 13-19.

Iwasaki, T., H. Hori, Y. Hayashi, T. Nishino, K. Tamura, S. Oue, T. Iizuka, T. Ogura and H. Esumi (1999). "Characterization of mouse nNOS2, a natural variant of neuronal nitric-oxide synthase produced in the central nervous system by selective alternative splicing." J Biol Chem 274(25): 17559-17566.

Jalowy, A., R. Schulz, H. Dorge, M. Behrends and G. Heusch (1998). "Infarct size reduction by AT1-receptor blockade through a signal cascade of AT2-receptor activation, bradykinin and prostaglandins in pigs." J Am Coll Cardiol 32(6): 1787-1796.

Jin, C. Z., J. H. Jang, H. J. Kim, Y. Wang, I. C. Hwang, S. Sadayappan,

B. M. Park, S. H. Kim, Z. H. Jin, E. Y. Seo, K. H. Kim, Y. J. Kim, S. J. Kim and Y. H. Zhang (2013). "Myofilament Ca2+ desensitization mediates positive lusitropic effect of neuronal nitric oxide synthase in left ventricular myocytes from murine hypertensive heart." J Mol Cell Cardiol 60: 107-115.

Jin, C. Z., J. H. Jang, Y. Wang, J. G. Kim, Y. M. Bae, J. Shi, C. R. Che, S. J. Kim and Y. H. Zhang (2012). "Neuronal nitric oxide synthase is up-regulated by angiotensin II and attenuates NADPH oxidase activity and facilitates relaxation in murine left ventricular myocytes." J Mol Cell Cardiol 52(6): 1274-1281.

Jones, E. S., A. Vinh, C. A. McCarthy, T. A. Gaspari and R. E. Widdop (2008). "AT2 receptors: functional relevance in cardiovascular disease." Pharmacol Ther 120(3): 292-316.

Kameya, S., Y. Miyagoe, I. Nonaka, T. Ikemoto, M. Endo, K. Hanaoka, Y. Nabeshima and S. Takeda (1999). "alpha1-syntrophin gene disruption results in the absence of neuronal-type nitric-oxide synthase at the sarcolemma but does not induce muscle degeneration." J Biol Chem 274(4): 2193-2200.

Katholi, R. E. and D. M. Couri (2011). "Left ventricular hypertrophy: major risk factor in patients with hypertension: update and practical clinical applications." Int J Hypertens 2011: 495349.

Kinugawa, S., H. Huang, Z. Wang, P. M. Kaminski, M. S. Wolin and T. H. Hintze (2005). "A defect of neuronal nitric oxide synthase increases xanthine oxidase-derived superoxide anion and attenuates the control of myocardial oxygen consumption by nitric oxide derived from endothelial nitric oxide synthase." Circ Res 96(3): 355-362.

Ladurner, A., C. A. Schmitt, D. Schachner, A. G. Atanasov, E. R. Werner, V. M. Dirsch and E. H. Heiss (2012). "Ascorbate stimulates endothelial nitric oxide synthase enzyme activity by rapid modulation of its phosphorylation status." Free Radic Biol Med 52(10): 2082-2090.

Lee, M. A., L. Cai, N. Hubner, Y. A. Lee and K. Lindpaintner (1997). "Tissue- and development-specific expression of multiple alternatively spliced transcripts of rat neuronal nitric oxide synthase." J Clin Invest 100(6): 1507-1512.

Lu, D., Y. Fu, A. Lopez-Ruiz, R. Zhang, R. Juncos, H. Liu, R. D. Manning, Jr., L. A. Juncos and R. Liu (2010). "Salt-sensitive splice variant of nNOS expressed in the macula densa cells." Am J Physiol Renal Physiol 298(6): F1465-1471.

Matter, C. M., L. Mandinov, P. A. Kaufmann, G. Vassalli, Z. Jiang and O. M. Hess (1999). "Effect of NO donors on LV diastolic function in patients with severe pressure-overload hypertrophy." Circulation 99(18): 2396-2401.

Mungrue, I. N. and D. S. Bredt (2004). "nNOS at a glance: implications for brain and brawn." J Cell Sci 117(Pt 13): 2627-2629.

Nguyen Dinh Cat, A., A. C. Montezano, D. Burger and R. M. Touyz (2013). "Angiotensin II, NADPH oxidase, and redox signaling in the vasculature." Antioxid Redox Signal 19(10): 1110-1120.

Niu, X., V. L. Watts, O. H. Cingolani, V. Sivakumaran, J. S. Leyton-Mange, C. L. Ellis, K. L. Miller, K. Vandegaer, D. Bedja, K. L. Gabrielson, N. Paolocci, D. A. Kass and L. A. Barouch (2012). "Cardioprotective effect of beta-3 adrenergic receptor agonism:

role of neuronal nitric oxide synthase." J Am Coll Cardiol 59(22): 1979-1987.

Oyamada, S., C. Bianchi, S. Takai, M. P. Robich, R. T. Clements, L. Chu and F. W. Sellke (2010). "Impact of acute myocardial ischemia reperfusion on the tissue and blood-borne renin-angiotensin system." Basic Res Cardiol 105(4): 513-522.

Padia, S. H. and R. M. Carey (2013). "AT2 receptors: beneficial counter-regulatory role in cardiovascular and renal function." Pflugers Arch 465(1): 99-110.

Patel, K. P. and H. D. Schultz (2013). "Angiotensin peptides and nitric oxide in cardiovascular disease." Antioxid Redox Signal 19(10): 1121-1132.

Paulus, W. J. (2000). "Beneficial effects of nitric oxide on cardiac diastolic function: 'the flip side of the coin'." Heart Fail Rev 5(4): 337-344.

Paulus, W. J., P. J. Vantrimpont and A. M. Shah (1994). "Acute effects of nitric oxide on left ventricular relaxation and diastolic distensibility in humans. Assessment by bicoronary sodium nitroprusside infusion." Circulation 89(5): 2070-2078.

Percival, J. M., K. N. Anderson, P. Huang, M. E. Adams and S. C. Froehner (2010). "Golgi and sarcolemmal neuronal NOS differentially regulate contraction-induced fatigue and vasoconstriction in exercising mouse skeletal muscle." J Clin Invest 120(3): 816-826.

Petroff, M. G., S. H. Kim, S. Pepe, C. Dessy, E. Marban, J. L. Balligand and S. J. Sollott (2001). "Endogenous nitric oxide

mechanisms mediate the stretch dependence of Ca2+ release in cardiomyocytes." Nat Cell Biol 3(10): 867-873.

Post, H., R. Schulz, P. Gres and G. Heusch (2001). "No involvement of nitric oxide in the limitation of beta-adrenergic inotropic responsiveness during ischemia." Am J Physiol Heart Circ Physiol 281(6): H2392-2397.

Putzke, J., B. Seidel, P. L. Huang and G. Wolf (2000). "Differential expression of alternatively spliced isoforms of neuronal nitric oxide synthase (nNOS) and N-methyl-D-aspartate receptors (NMDAR) in knockout mice deficient in nNOS alpha (nNOS alpha(Delta/Delta) mice)." Brain Res Mol Brain Res 85(1-2): 13-23.

Ramchandran, R., T. Takezako, Y. Saad, L. Stull, B. Fink, H. Yamada, S. Dikalov, D. G. Harrison, C. Moravec and S. S. Karnik (2006). "Angiotensinergic stimulation of vascular endothelium in mice causes hypotension, bradycardia, and attenuated angiotensin response." Proc Natl Acad Sci U S A 103(50): 19087-19092.

Ritter, O., K. Schuh, M. Brede, N. Rothlein, N. Burkard, L. Hein and L. Neyses (2003). "AT2 receptor activation regulates myocardial eNOS expression via the calcineurin-NF-AT pathway." FASEB J 17(2): 283-285.

Sartoretto, J. L., H. Kalwa, M. D. Pluth, S. J. Lippard and T. Michel (2011). "Hydrogen peroxide differentially modulates cardiac myocyte nitric oxide synthesis." Proc Natl Acad Sci U S A 108(38): 15792-15797.

Sears, C. E., S. M. Bryant, E. A. Ashley, C. A. Lygate, S. Rakovic, H. L. Wallis, S. Neubauer, D. A. Terrar and B. Casadei (2003). "Cardiac neuronal nitric oxide synthase isoform regulates

myocardial contraction and calcium handling." Circ Res 92(5): e52-59.

Smith, C., M. Merchant, A. Fekete, H. L. Nyugen, P. Oh, Y. L. Tain, J. B. Klein and C. Baylis (2009). "Splice variants of neuronal nitric oxide synthase are present in the rat kidney." Nephrol Dial Transplant 24(5): 1422-1428.

Sun, J., E. Picht, K. S. Ginsburg, D. M. Bers, C. Steenbergen and E. Murphy (2006). "Hypercontractile female hearts exhibit increased S-nitrosylation of the L-type Ca2+ channel alpha1 subunit and reduced ischemia/reperfusion injury." Circ Res 98(3): 403-411.

Takimoto, E., H. C. Champion, M. Li, S. Ren, E. R. Rodriguez, B. Tavazzi, G. Lazzarino, N. Paolocci, K. L. Gabrielson, Y. Wang and D. A. Kass (2005). "Oxidant stress from nitric oxide synthase-3 uncoupling stimulates cardiac pathologic remodeling from chronic pressure load." J Clin Invest 115(5): 1221-1231.

Takimoto, Y., T. Aoyama, K. Tanaka, R. Keyamura, Y. Yui and S. Sasayama (2002). "Augmented expression of neuronal nitric oxide synthase in the atria parasympathetically decreases heart rate during acute myocardial infarction in rats." Circulation 105(4): 490-496.

Tambascia, R. C., P. M. Fonseca, P. D. Corat, H. Moreno, Jr., M. J. Saad and K. G. Franchini (2001). "Expression and distribution of NOS1 and NOS3 in the myocardium of angiotensin II-infused rats." Hypertension 37(6): 1423-1428.

Ueda, K., C. Valdivia, A. Medeiros-Domingo, D. J. Tester, M. Vatta, G. Farrugia, M. J. Ackerman and J. C. Makielski (2008). "Syntrophin mutation associated with long QT syndrome through activation of

the nNOS–SCN5A macromolecular complex." Proc Natl Acad Sci U S A 105(27): 9355–9360.

Unger, T. (2002). "The role of the renin–angiotensin system in the development of cardiovascular disease." Am J Cardiol 89(2A): 3A–9A; discussion 10A.

Varagic, J. and E. D. Frohlich (2002). "Local cardiac renin–angiotensin system: hypertension and cardiac failure." J Mol Cell Cardiol 34(11): 1435–1442.

Wiemer, G., G. Itter, T. Malinski and W. Linz (2001). "Decreased nitric oxide availability in normotensive and hypertensive rats with failing hearts after myocardial infarction." Hypertension 38(6): 1367–1371.

Witt, C. C., C. Burkart, D. Labeit, M. McNabb, Y. Wu, H. Granzier and S. Labeit (2006). "Nebulin regulates thin filament length, contractility, and Z–disk structure in vivo." EMBO J 25(16): 3843–3855.

Xu, K. Y., D. L. Huso, T. M. Dawson, D. S. Bredt and L. C. Becker (1999). "Nitric oxide synthase in cardiac sarcoplasmic reticulum." Proc Natl Acad Sci U S A 96(2): 657–662.

Yang, X. P., Y. H. Liu, E. G. Shesely, M. Bulagannawar, F. Liu and O. A. Carretero (1999). "Endothelial nitric oxide gene knockout mice: cardiac phenotypes and the effect of angiotensin–converting enzyme inhibitor on myocardial ischemia/reperfusion injury." Hypertension 34(1): 24–30.

Zhang, X., C. Dong, Q. J. Wu, W. E. Balch and G. Wu (2011). "Di–acidic motifs in the membrane–distal C termini modulate the

transport of angiotensin II receptors from the endoplasmic reticulum to the cell surface." J Biol Chem 286(23): 20525-20535.

Zhang, Y. H. and B. Casadei (2012). "Sub-cellular targeting of constitutive NOS in health and disease." J Mol Cell Cardiol 52(2): 341-350.

Zhang, Y. H., L. Dingle, R. Hall and B. Casadei (2009). "The role of nitric oxide and reactive oxygen species in the positive inotropic response to mechanical stretch in the mammalian myocardium." Biochim Biophys Acta 1787(7): 811-817.

Zhang, Y. H., C. Z. Jin, J. H. Jang and Y. Wang (2014). "Molecular mechanisms of neuronal nitric oxide synthase in cardiac function and pathophysiology." J Physiol 592(15): 3189-3200.

Zhang, Y. H., M. H. Zhang, C. E. Sears, K. Emanuel, C. Redwood, A. El-Armouche, E. G. Kranias and B. Casadei (2008). "Reduced phospholamban phosphorylation is associated with impaired relaxation in left ventricular myocytes from neuronal NO synthase-deficient mice." Circ Res 102(2): 242-249.

국문 초록

심근세포에 발현된 nNOS는 수축과 세포 내 칼슘 조절에 관여한다. 고혈압 쥐 심근에서 nNOS 단백질의 발현 증가는 심근세포 의 미세근섬유 칼슘 민감성을 감소시켜 이완을 촉진하며, 이는 압력과부하 방지 역할을 한다. 하지만 nNOS 단백질의 증가 조절 기전 및 nNOS에 의한 근미세섬유 조절 기전의 세부 연구는 여전히 부족하다. 과잉 분비 시 고혈압을 일으키는 안지오텐신 II는 제1형 수용체(AT1R)를 통하여 NADPH 산화효소 (NOX) 활성화 및 다양한 병리적 신호를 일으킨다. 백서 심근세포에 안지오텐신 II 투여는 nNOS 발현을 높이는데, 불과 30분만에 NOX를 매개로 활성산소 증가 및 제2형 수용체(AT2R)의 세포막 이동-발현을 유발한다. 본 연구를 통하여 Ang II 자극 시 활성산소 증가는 eNOS 활성화를 유도하는 것을 발견하였다. 이에 의한 NO증가가 AT2R 단백질 C-말단 부분의 시스테인 349번 잔기 나이트로실화를 일으키며, 이에 따라 세포막 이동-발현이 유도되고, AT2R 자극은 nNOS 발현 증가를 일으켰다. eNOS 억제 혹은 유전자 결핍은 안지오텐신 II에 의한 nNOS 발현을 차단하였기에 이는 그 중요성을 시사한다. 다음 연구로, 근미세섬유에 작용하는 nNOS의 역할 및 고혈압의 병태생리에서 변화를 알아보았다. nNOS 억제제를 지속적으로 투여한 쥐에 안지오텐신 II를 4주간 추가

주입한 경우, 안지오텐신 II만 주입하였을 경우보다 혈압 증가가 심했고, 좌심실비대 및 심근섬유화가 관찰되었다. nNOS 억제 쥐의 심실근세포는 근절길이와 I-band 길이가 증가하였다. 전기적 자극으로 심실근세포 수축을 유발하면서 칼슘농도 변화를 동시에 측정해 보면, nNOS 억제 심실근세포는 안지오텐신 II 투여에 관계없이 이완기 칼슘농도와 근미세섬유 칼슘 민감성이 함께 증가하였다. 이는 nNOS가 근섬유 구조 유지와 칼슘 의존적 수축조절에 필수적임을 시사하며, 고혈압 조건에서 심근비대 방지에도 중요한 것으로 보인다. 지금까지 간과되었던, 심실근세포 내 nNOS 접합변이체들의 분포를 조사하였다. 흥미롭게도, 세포질과 세포막 분획에는 nNOSα/μ가 풍부한 반면, 보다 작은 분자량을 가진 nNOSβ는 근섬유 분획에서 새롭게 발견되었다. nNOSα/μ 유전자가 결손된 쥐의 근섬유 분획에서 nNOSα/μ발현이 여전히 관찰되며 이 심실근세포의 근절길이, I-band, 굵은 필라멘트의 길이 등 구조는 정상이었다. 심근세포에서 이른 시간에 유도되는 활성산소에 의한 eNOS 활성화는 AT2R의 나이트로실화 현상을 가속화시켜 세포막으로의 AT2R이동을 증가시키고, 궁극적으로 안지오텐신 II 자극에 의한 nNOS단백질의 발현을 증가시킴을 알 수 있었다. 또한, nNOS가 갖는 새로운 기능으로써 근섬유 구조 유지 기능이 있음을 확인하였을 뿐 아니라, 미세근섬유 분획에서 새로운 nNOS 아형인 nNOSβ가 존재함을 처음으로

보았다. nNOSβ의 분포는 근섬유 및 근절 구조 유지에 핵심적인 것으로 해석된다. 따라서, 기존에 알려진 nNOS의 이완기 칼슘 조절 기능과 더불어 nNOSβ의 심근비대 방지 역할을 새로운 가설로 제안한다.

본 내용의 일부는 *Basic Res Cardiol* (2015) 110(3):21. 와 *Nitric Oxide* (2015) 11;50:20-27. 학술지에 출판 완료되었다.

주요어: 신경형산화질소 (nNOS), 심근섬유, 안지오텐신 II, 심근비대
학 번: 2013-30617